Shi *et al. Cell Communication and Signaling* (2025) 23:141
https://doi.org/10.1186/s12964-025-02116-z

Cell Communication and Signaling

RESEARCH Open Access

Increased melanin induces aberrant keratinocyte – melanocyte – basal – fibroblast cell communication and fibrogenesis by inducing iron overload and ferroptosis resistance in keloids

Xiangguang Shi[1,6,7,8†], Xueyi Xia[2†], Yang Xiao[2†], Ying Zhang[1†], Yiyi Gong[1], Yahui Chen[2], Chenyi Shi[2], Wei Wang[2], Jianlan Liu[1], Jia Huang[1], Mengguo Liu[1], Zhuoya Xu[2], Yanyun Ma[2], Mengkun Shi[3*], Jiucun Wang[1,2,4,5*] and Wenyu Wu[1,6,7,8*]

Abstract

Background Keloid is a typical skin fibrotic disease with unclear mechanisms and limited therapeutic options. Fibroblast-induced fibrogenesis is a crucial cause of KD. However, the types of cells involved in fibroblast fibrogenesis in KD and the specific mechanisms are unclear. This study aimed to investigate the role of melanocyte-secreted melanin in promoting fibroblast fibrogenesis and its mechanism and to evaluate the potential therapeutic effect of intervening melanin in treating keloid.

Methods The activity of pigmentation-related pathways in KD melanocytes was examined using single-cell RNA-sequence (scRNA-seq) analysis. Masson-Fontana staining or isolated melanin quantification detected the melanin levels and distribution in the skin and cells. Collagen deposition, wounding healing, and proliferation analysis were employed to integratively assess fibroblast fibrogenesis. After melanin treatment, bulk-seq identified fibroblasts' differentially expressed genes (DEGs). The iron levels were detected by Perl's staining or isolated iron quantification. Cell viability, LipidROS, and malondialdehyde assay accessed the ferroptosis levels. The therapeutic potential of ML329 was evaluated in keloid-bearing mice.

†Xiangguang Shi, Xueyi Xia, Yang Xiao and Ying Zhang contributed equally to this work.

*Correspondence:
Mengkun Shi
9450@huashan.org.cn
Jiucun Wang
jcwang@fudan.edu.cn
Wenyu Wu
wuwenyu@huashan.org.cn

Full list of author information is available at the end of the article

Results We found the enriched skin pigmentation-related pathways in the melanocytes of keloid by single-cell RNA-sequence (scRNA-seq) analysis. We further validated increased melanin levels in keloid patients. Additionally, melanin positively correlated with the Keloid Area and Severity Index in keloid. Furthermore, melanocyte-secreted melanin significantly promoted fibroblast proliferation, migration, and collagen synthesis. Mechanically, melanin increased basal cell permeability and inflammation to facilitate its transfer to the dermis, where it further activated fibroblasts by evoking iron overload and ferroptosis resistance. Consistently, iron overload and ferroptosis resistance were validated in primary fibroblasts and skin tissues of keloid patients. Inhibition of iron overload and ferroptosis resistance effectively diminish melanin-induced fibrogenesis. Interestingly, melanin induced iron overload and ferroptosis resistance in melanocytes in an autocrine manner and further stimulated keratinocytes to take up melanin to deepen skin color by upregulating the F2R-like trypsin receptor 1 (F2RL1). In vivo, the delivery of ML329, a microphthalmia-associated transcription factor (MITF) inhibitor, could suppress melanogenesis and alleviate keloid in human keloid-bearing nude mice. Meanwhile, ML329 decreased the iron content and restored the sensitivities of ferroptosis.

Conclusion Collectively, melanin-lowing strategies may appear as a potential new therapeutic target for keloid.

Graphical abstract

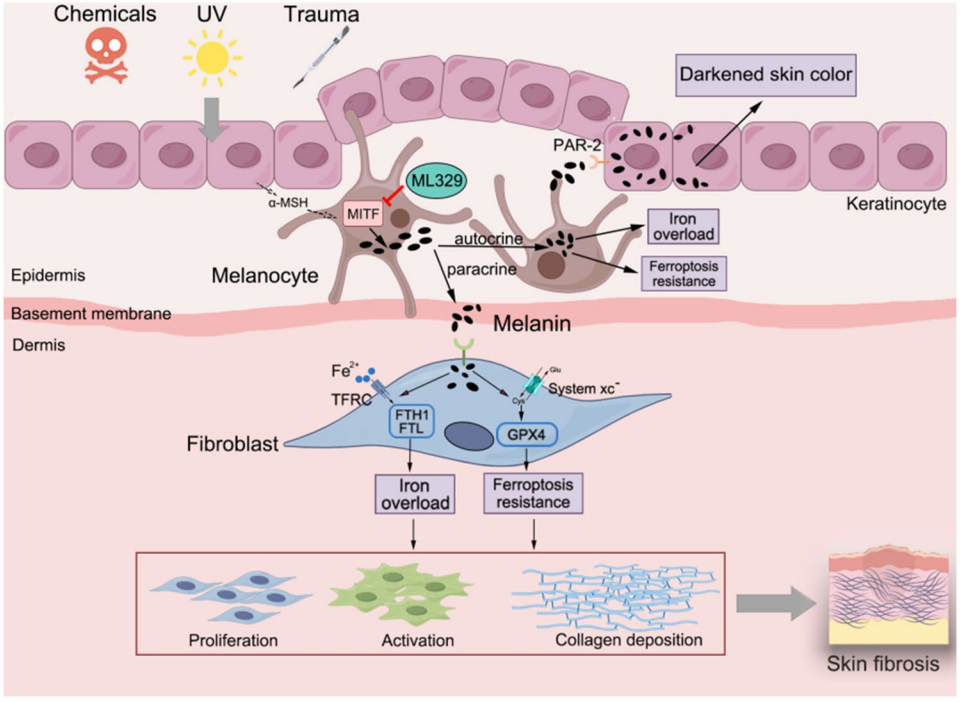

In Brief

Current treatments for keloid are ineffective. Our research demonstrates that melanin levels increase in keloid patients and play a significant role in keloid progression by mediating aberrant keratinocyte – melanocyte – basal – fibroblast cell crosstalk. Importantly, we found that pharmacological inhibition of melanogenesis using an MITF inhibitor, ML329, shows promise in effectively alleviating keloid, offering a potential breakthrough in keloid treatment.

Highlights

- The melanin synthesis pathway is abnormally activated in KD melanocytes.
- Melanin destroys the basal membrane barrier by triggering inflammation and translocates to the dermal layers of the skin in a paracrine manner to induce fibroblast overgrowth, migration, and ECM deposition by inducing iron overload and ferroptosis resistance.
- Melanin maintains melanocytes' hyperproliferative and non-immortal properties in an autocrine manner. It further enhances the keratocyte PAR-2 to promote transit to the superficial epidermis skin layers, which may be related to the deepening of skin color.
- Inhibition of melanin synthesis by ML329 alleviates KD in mice.

Keywords Keloid, Melanin, Fibrogenesis, Iron overload, Ferroptosis resistance

Background

Keloid (KD) has the characteristics of tumor growth, manifested as continuous scar hyperplasia beyond the edge of the wound [1]. Keloid is a pathological scar formed by excessive proliferation of fibroblasts and excessive extracellular matrix deposition in skin wound repair. It affects the appearance and is often accompanied by itching and pain, seriously affecting patients' quality of life [2–4]. In routine wound healing, collagen anabolism and degradation metabolism maintenance are balanced. However, this average balance is disrupted in keloids, and collagen synthesis significantly outstrips degradation, ultimately leading to a massive buildup of collagen, although the exact cause of this change is unknown. The pathogenesis of keloid is complex, and the FDA or CFDA currently approves no drug.

Multiple factors are involved in keloid formation, including abnormal wound healing, excessive tension, immune disorders, and hormonal imbalances [1]. Previous single-cell studies also found that various cell types in skin tissue, including dermal fibroblasts, macrophages, endothelial cells, and other types of cells, are widely involved in keloid formation [5–9]. It is important to note that the prevalence and recurrence of keloids vary significantly by ethnicity, with relatively high rates in people of Asian or African descent. At the same time, the incidence reported in Caucasian populations is less than 1% [10, 11]. Overall, the incidence of keloids is 6 to 9 times higher in dark-skinned people than in light-skinned people [12]. Furthermore, people with albinism of all races could not develop into keloid, including black people. These shreds of evidence strongly suggest that cellular abnormalities related to melanin metabolism may be involved in the occurrence and development of scars.

Melanogenesis is a biosynthetic pathway for melanin production in melanocytes, involving a complex series of enzyme-catalyzed and chemically-catalyzed reactions [13]. Five signaling pathways are involved in regulation, of which Microphthalmia-associated transcription factor (MITF) is an essential target of each path [14]. Melanosomes are specific sites for melanin synthesis, located within melanocytes, which are located at the base level of the human epidermis, with many bumps called dendrites on the cell surface [15]. When challenged with ultraviolet radiation, melanocytes synthesize melanin in melanosomes and pass it to keratinocytes through dendrites. The melanin synthesis process is highly complex and mainly involves tyrosinase (TYR), tyrosinase-related protein 1 (Tyrosinase-related protein-1, TRP-1), and tyrosinase-related protein-2 (TRP-2) [16]. Pmel17 (gp100) is a structural protein of melanosomes essential for forming the internal fibrous matrix characteristics of phase II melanosomes [17]. Melanosome formation is a critical step in melanism, but melanosomes must be transferred from melanocytes to keratinocytes to promote melanin production. Proteinase-activating receptor (PAR)-2 induces melanosome transfer by increasing the phagocytosis of melanosomes by keratinocytes. Ultraviolet radiation stimulates PAR-2 expression and induces melanosome transfer by inhibiting keratinocyte receptor-proteinase-activating receptor 2, a potential mechanism for regulating pigmentation [18, 19]. Studies have shown that melanin content increased in KD skin tissue and positively correlated with collagen expression [20]. Besides, there was a relationship between skin color and keloid [21]. The study also reported elevated tyrosinase activity and expression of the transcription factor MITF in KD melanocytes [22]. Moreover, melanocytes can activate fibroblast collagen synthesis by secreting exosomal microRNA [22]. Although evidence suggests that melanocytes may be involved in the occurrence and development of KD, the exact role and mechanism of melanocytes, especially the role and mechanism of melanin in KD, remain largely unknown.

Iron metabolism plays a vital role in maintaining skin homeostasis [23]. Iron production, transport, absorption, and excretion are in a dynamic balance in the body, thus supporting various biochemical catalytic reactions, hemoglobin synthesis, and various physiological functions. Iron deficiency can cause anemia, and iron overload can cause hemochromatosis. Iron also causes the peroxidation of polyunsaturated phospholipids through the Fenton reaction to produce excessive Lipidros, which eventually causes ferroptosis. Iron metabolism disorders and their secondary ferroptosis regulation abnormalities are involved in the occurrence and development of various skin diseases. Ming Zhao et al. reported that Iron-dependent epigenetic modulation promotes pathogenic T-cell differentiation in lupus [24]. Iron overload and ferroptosis also contribute to the formation of skin lesions in psoriasis [25], melanoma [26], scleroderma [27], psoriasis [28], etc. In addition, iron overload and ferroptosis are also widely involved in various skin physiological regulations such as wound healing, skin injury, inflammation, immunity, skin aging, and skin barrier [29]. Targeting iron metabolism and ferroptosis regulation has been recognized as a promising therapeutic strategy for skin-related diseases. However, whether iron metabolism and ferroptosis are abnormal in KD, the mode of regulation, and their role in KD is unknown. Further exploration of the mechanism of iron metabolism and ferroptosis in KD and developing intervention strategies based on iron metabolism and ferroptosis will significantly contribute to diagnosing and treating KD.

In this study, we found that the melanogenesis signaling pathway is abnormally activated in KD melanocytes, resulting in a significant increase in melanin content in KD. The over-secreted melanin promotes fibroblast

proliferation, migration, and collagen deposition through iron overload and also endorses fibroblasts with ferroptosis resistance, thereby maintaining fibroblast hyperplasia. In addition, melanocytes secreted melanin inhibits the ferroptosis of melanocytes themselves in an autocrine manner, and melanocytes with ferroptosis resistance can promote the expression of melanin receptors of keratinocytes, thereby promoting the transfer of melanin to keratinocytes. Inhibition of melanin synthesis in melanocytes effectively reduced keloid formation in human keloid-bearing nude mice. Taken together, we discovered the critical role of melanin in keloid. The treatment of KD will benefit by inhibiting melanin secretion and blocking iron overload and ferroptosis resistance caused by melanin.

Materials and methods

Patients

According to the JSW Scar Scale (JSS) 2015 classification and evaluation standards, the skin samples utilized in this study were taken from keloid patients at Shanghai Huashan Hospital [30]. Paired keloids refer to normal skin tissue (KN) surrounding the keloid (KD) tissue on the same patient that was taken at the same time during the surgery. These KN and KD tissues are described as paired tissues. Unpaired tissues are those where only KD or normal skin tissue was taken during the surgery, which did not originate from the same person. Notably, the control paired KN samples were taken from the appropriately region-matched keloid. Before beginning, all participants were fully informed about the study and given their informed consent. The Keloid Area and Severity Index (KASI) was investigated in compliance with previous studies [31]. The ethics council at Fudan University authorized the research, and further details on the patients and normal controls may be seen in Supplementary Table S1.

Melanin measurement

As previously mentioned, spectrophotometric measurement of melanin was done [32]. Briefly, trypsin incubation, inactivation, and centrifugation were used to extract cell pellets from a 10 mg skin tissue single-cell suspension. The pellets were then frozen at -20 °C before being measured. Samples were then made soluble by adding 1 M NaOH and 10% DMSO and letting them sit at 80 °C for 30 min. Ultimately, a plot of absorbance at 490 nm was created, and the standard curve was used to determine concentration.

Perl's staining and iron assay

As directed by the manufacturer, Perl's staining was carried out (Hematognost Fe®, 112,084, Sigma-Aldrich, St. Louis, MO, USA). After 5% potassium hexacyanoferrate and 5% hydrochloric acid were added to the slices, 0.1% nuclear fast red was used as a counterstain. Slices were photographed using light microscopy (NIKON ECLIPSE C1) after being cleaned in distilled water, dehydrated in a sequence of increasing alcohol concentrations, and cover-slipped. Total iron, Fe^{2+}, and Fe^{3+} levels in cultured cells or skin tissues were determined using an iron assay kit from Dojindo (cat. no. I291, Iron Assay Kit -Colorimetric), according to the manufacturer's instructions. The absorbance of each sample was measured at 593 nm using a Multiskan GO Microplate Spectrophotometer (Thermo Fisher Scientific, Inc.).

Cell cultures

The isolation of dermal primary fibroblasts from keloid patients and normal controls was carried out as previously described [20]. Briefly, skin biopsy specimens were cleaned in 75% ethanol and washed three times in phosphate-buffered saline (PBS) containing streptomycin and penicillin. The specimens of the corium layer were cut into particles and then placed in culture dishes. After two hours of inverse culture, DMEM was added for cell culture. Primary dermal fibroblasts from the third and fifth passages were used for additional analysis. Primary human epidermal melanocytes were purchased from ATCC and were isolated from the skin of an adult donor (cat. No. PCS-200-013™). The adult melanocytes were cultured using a growth kit containing 5 μg/mL rh Insulin, 50 μg/mL ascorbic acid, 6 mM L-glutamine, 1.0 μM epinephrine, 1.5 mM calcium chloride, peptide growth factor supplement. The human skin basal cell line TE354T was cultured in DMEM containing 10% FBS. The HaCaT cells were cultured in the medium containing 89% MEM, 10% fetal bovine serum superior, 1% dual antibody, and 0.2% bovine pituitary extract.

Cell permeability

200 ul of endothelial cells TE 354.T suspension were seeded on a Transwell chamber with 0.4 μm pore PTFE membrane (Corning Costar Corp, Acton, MA) at a density of 10^5 cells/cm^2. The chamber was then embedded in a 12-well plate with 500 ul medium. The cells were allowed to grow for 4–5 days until the cells reached 100% confluence and formed mature monolayers. The medium was removed from the chamber and plate and washed with phosphate-buffered saline (PBS) 3 times. After that, 200 ul phenol red-containing DMEM with melanin or saline was added into the chamber, while the subjacent plate was added 500 ul DMEM without phenol red. 4 h later, 200 ul medium was from the plate and the absorbance at 430 nm with a microplate reader.

Establishment of the human keloid-bearing mouse model

The Institutional Animal Care and Use Committee of Fudan University approved the standards that were followed when using Balb/c nude mice in this investigation. Keloid biopsy specimens had their dermis cut into 5 mm cubes and kept at comparable weights. Six to eight-week-old nude mice were given 1.25% tribromoethanol as anesthesia before one cube was inserted into a 1-centimeter incision on the skin just below the right shoulder blade in order to implant the keloid tissues. Next, the wound was sutured. After being housed separately under usual settings for 14 days, these mice, which carried keloids, were ready for the next round of trials. For keloid treatment, keloid-bearing mice received 5 mg/kg ML329 injections once every three days for eight times total until harvested.

Histological and immunofluorescence detection

Prior to being embedded in paraffin for hematoxylin and eosin (H&E), Masson's staining, Masson-Fontana staining, and immunofluorescence (IF) staining, the keloid and adjacent normal tissue samples were first preserved in 10% paraformaldehyde. The standard operating procedures were followed for Masson's staining, Masson-Fontana staining, and H&E. In order to perform IHC staining and IF staining, samples were first incubated with primary antibodies, including anti-α-S100A4 (1:100), anti-MITF (1:100), and anti-COL17A1 (1:100), and the samples were subsequently incubated with either the FITC conjugated Anti-Mouse (1:100) or Cy3 conjugated Anti-Rabbit (1:100) second antibody. Hematoxylin was used as a counterstain, and DAB peroxidase substrate was used to view the IHC sections. DAPI was used to counterstain the IF sections and the nuclei. A NIKON ECLIPSE C1 was used to take fluorescence confocal pictures.

RNA isolation, cDNA synthesis, and real-time qRT-PCR

Using an RNA Isolation Kit, the total RNA of keloid and normal control primary fibroblast from the third to fifth passages and skin tissues was isolated in accordance with the manufacturer's protocol. Reverse transcriptase was used to synthesize cDNA using a HiScript II 1st Strand cDNA Synthesis Kit. Using the SYBR-Green-based approach, real-time qRT-PCR was carried out using a Roch-LC480 Real-Time PCR system (Roche, Switzerland). Supplementary Table S2 provides a description of primer sequences. The expression of each gene was compared to β-actin or GAPDH.

ELISA

The protein levels of CCL2 (EZMCP1, Sigma), Calprotectin (S100A8/S100A9, Abcam, ab320045, Cambridge, MA, USA), c-Kit (ab45924, Abcam), IL-4(ab215089, Abcam), and TNF-α (ab181421, Abcam) were measured using the ELISA kits following the manufacturer's instructions.

Protein extraction and Western blot

Protein extraction of primary fibroblasts and skin tissues from keloid and normal controls was performed following the manufacturer's instructions. Next, total proteins were separated using 10% SDS-PAGE electrophoresis and then placed onto Millipore 0.45 μm nitrocellulose membranes. After blocking with 5% BSA/TBST solution, the primary antibodies were incubated for an additional night at 4 °C. Afterward, the secondary antibodies with HRP conjugation were added. Primary antibodies used in western blot analysis were anti-collagen type I antibody (A22090, ABclonal), anti-α-SMA antibody (GB111364, Servicebio), anti-Ferritin antibody (4393 S, CST), anti-GPX4 antibody (67763-1-Ig, Proteintech), anti-SLC3A2 antibody (4511 S, Proteintech), anti-SLC7A11 antibody (26864-1-AP, Proteintech), anti-SLC40A1 antibody (NBP1-21502, NOVUS), anti-TFRC antibody (ab214039, Abcam), anti-ACSL4 antibody (ab155282, Abcam) and F2RL1antibody (ab184673, Abcam), and anti-MITF antibody (ab303530, Abcam). Every experiment was carried out three independently times. The expression of each protein was compared to β-actin or GAPDH. **Supplementary Files** contained uncropped western blots.

Cell viability and proliferation assay

Cell viability was assessed using CCK-8. Briefly, fibroblast or melanocyte cells (1×10^4 cells/well) were cultured in 96-well culture plates for 24 h. After removing the culture medium, RSL-3 was added and incubated for another 24 h. Before CCK8 analysis, ten μL of CCK-8 solution was added to each well. Following two hours of incubation, absorbance was measured on a microplate spectrophotometer at a wavelength of 450 nm. Cell proliferation was measured by using a cell counter. Briefly, after giving the cells with PBS wash, trypsin was added to digest cells, and the reaction was terminated with culture media. Following a thorough suspension, samples were counted using a Countstar Mira FL (Alit Biotech (Shanghai) Co., Ltd.).

Transwell co-culture assay

The Transwell co-culture assay was performed in a 12-well plate. The pHEMs are placed into the insert with 0.4 μm pores, and the HaCaT cells were sed in the plate. After co-culture for 48 h, the HaCaT cells were collected and melanin content was assessed.

MDA, 4-HNE, and lipidros assay

MDA and 4-HNE were measured with a lipid peroxidation (MDA) assay kit (M496, Dojindo Laboratories, Kumamoto, Japan) and lipid peroxidation (4-HNE) assay

kit (ab238538, Abcam, Cambridge, England), respectively. Lipid peroxide was stained by Liperfluo (L248, Dojindo) according to the manufacturer's protocol. Liperfluo was added to the medium, and fibroblast cells were incubated at 37 °C for an hour. Fibroblasts were observed by fluorescent microscope (NIKON ECLIPSE C1).

Measurement of mitochondrial membrane potential (MMP) and MitoROS

Following the manufacturer's instructions as outlined in other investigations [33, 34], TMRM (T668, Invitrogen) and the mitoROS probe MitoSOX (M36008, Invitrogen) were utilized in live cells to measure the levels of MMP and mitochondrial ROS. MMP levels were quantitated by detecting 580 nm emission wavelength at 535 nm excitation wavelength, and the mitoROS levels were measured by detecting 580 nm emission wavelength at 510 nm excitation wavelength using a multimode reader.

Sircol assay

Using the Sircol assay kit and the manufacturer's instructions, the total soluble collagen content in the medium was measured, and the amount of collagen protein in the cell media was standardized to the total amount of protein.

RNA interference

The short interfering RNA (siRNA) sequences of MITF were synthesized from HANBIO. Sequences for *MITF* siRNAs are:

si-MITF forward 5′-GGACAAUCACAACCUGAUUTT-3′and.

si-MITF reverse 5′-AAUCAGGUUGUGAUUGUCCTT-3′.

Scrambled sequences: forward 5′-UUCUCCGAACGUGUCACGUTT-3′ and reverse 5′-ACGUGACACGUUCGGAGAATT-3′ were used as non-targeting control siRNA (NC). Using Lipofectamine™ RNAiMAX Transfection Reagent, 30 pmol of siRNA or NC were transfected into cells. Following a 48-hour of transfection, the cells were gathered for additional study.

Wound healing scratch assay

Fibroblasts were cultured in DMEM supplemented with 0.1% FBS in order to inhibit cell growth, and the fibroblasts were allowed to reach confluence before undergoing cell scratches as previous study [35]. By measuring the most significant distance between the two edges of the scratches, the degree of wound healing was ascertained. The assessment of migration rate was conducted by computing wound repairability using the following equation: wound repair = 100 × (A − B)/A, where A is the initial scratch width (0 h), and B is the scratch width after 24–36 h.

RNA sequencing (RNA-seq)

Total RNA extraction and cDNA library construction of fibroblast cells followed the manufacturer's instructions using a KAPA RNA HyperPrep kit (Kapa Biosystems, Wilmington, MA, USA). The Illumina HiSeq X Ten system (Illumina, USA) was utilized to sequence the cDNA libraries. Deseq2 and Kallisto performed the analysis on the transcriptome data. DEGs are defined as differentially expressed genes ($P < 0.05$).

Single-cell RNA-Seq (scRNA-seq)

Skin samples from six keloid patients (KD) and six neighboring skin subjects (KN) were PBS-washed, minced, and enzymatically dissociated. Epidermal and dermal layers were separated, further digested with trypsin or collagenase P/Dnase I, respectively, and filtered for single-cell suspensions. Single-cell reagent kits (3' v3; 10X Genomics) were used to prepare library samples after digestion. The 10X Genomics Chromium System was employed for scRNA-seq, with cell lysis, mRNA reverse transcription, barcoding, UMI attachment, cDNA amplification, and Illumina HiSeq 4000 sequencing. Cell clustering and the discovery of genes with differential expression were made after excluding cells based on mitochondrial gene count and gene expression range and applying Harmony for batch correction. UMAP visualized clusters after PCA, with marker genes identified by differential expression analysis.

CellChat analysis

The cell communication network of different cell types in normal and KD patients by CellChat (v1.6.1). The heatmap was applied to illustrate the differential quantity and strength of cell-cell interactions in KD patients compared to control samples. Dark red indicates elevated interaction, while blue indicates reduced interaction in KD compared to KN samples. We use CellChat with the function 'netVisual_heatmap' to show the differential number of interactions (Supplementary Figure S6A) or interaction strengths (pplementary Figure S6B) between pairs of KD and KN datasets in greater detail. In this heatmap, the top-colored bar plot represents the sum of each column of the absolute values displayed in the heatmap (incoming signaling). The right-colored bar plot represents the sum of each row of the absolute values (outgoing signaling). Therefore, the bar height indicates the degree of change regarding the number of interactions or strength between the two conditions. In the heatmap, the color of each cell indicates whether there is increased or decreased signaling in the second dataset compared to the first one, with dark red representing elevated

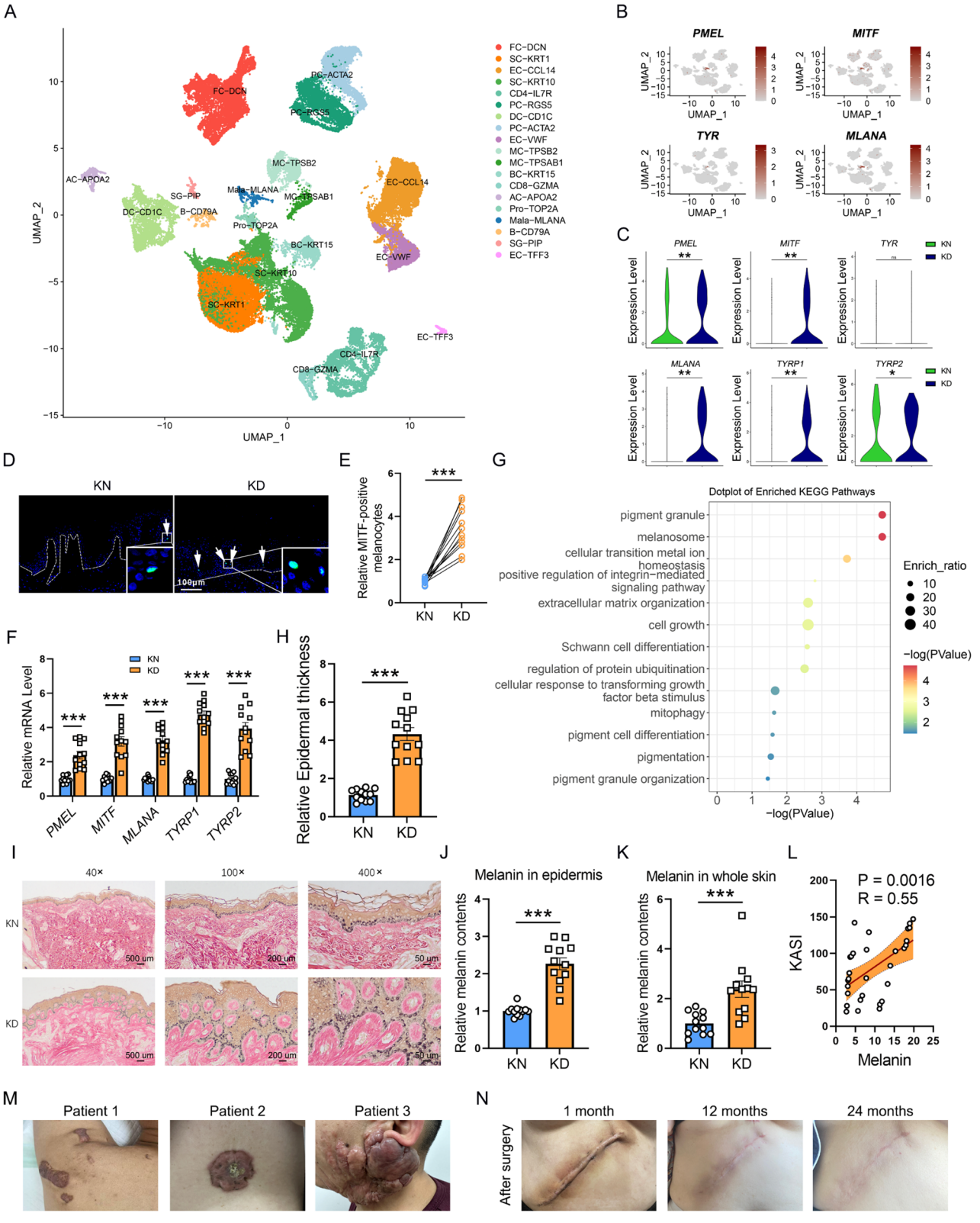

Fig. 1 (See legend on next page.)

(See figure on previous page.)

Fig. 1 Hyperactive pigmentation in melanocyte cells from KD patients. (**A**) UMAP of the cell clustering from skin tissues by scRNA-seq analysis. (**B**) Re-clustering of melanocytes by *PMEL*, *MITF*, *TYR*, and *MLANA*. (**C**) The mRNA levels of *PMEL*, *MITF*, *TYR*, and *MLANA* in KD and KN skin tissues by scRNA-seq analysis. (**D-E**) Immunofluorescence assay and cell count of MITF-positive melanocytes in epidermis of skins. The dashed white lines represent the epidermis above and the dermis below. $N = 12$. Scale bar: 100 μm. (**F**) *PMEL*, *MITF*, *MLANA*, *TYRP1*, *and TYRP2* levels in keloid skin tissues by quantitative Real-time PCR (qPCR) analysis. $N = 12$. (**G**) KEGG analysis of the Differentially Expressed Genes (DEGs) of melanocytes between KD and KN from scRNA-seq. (**H**) Epidermal dermal thickness changes between KD and KN skin tissues. (**I-J**) Masson-Fontana staining (I) and quantification (J) of melanin contents in skin epidermis. $N = 12$. 40×, 100×, and 400× means the images are magnified by 40, 100, and 400 times, respectively. Scale bar: 500 μm, 200 μm and 50 μm in 40×, 100× and 400×, respectively. (**K**) Quantifying isolated melanin from skin tissues by spectrophotometric measurement at 490 nm of absorbance. $N = 12$. (**L**) The correlations between KASI and melanin ($N = 30$). (**M-N**) The photos of keloid patients. $^{*}P < 0.05$; $^{**}P < 0.001$; $^{***}P < 0.001$

interaction and blue signifying reduced interaction in KD patients compared to KN samples.

Statistical analysis

Both the Shapiro-Wilk test and a visual inspection were used to determine normality. The independent sample t-test was used when the parameters had homogeneous variances and a normal distribution. On the other hand, a non-parametric Mann-Whitney test was applied if the variances were not homogeneous. P-values below 0.05 were regarded as significant.

Results

scRNA-seq analysis revealed enhanced pigmentation in melanocytes of keloid skin tissues and positively associated with disease severity and prognosis

To shed light on the pathophysiology of skin fibrosis, we performed single-cell RNA sequencing (scRNA-seq) on six pairs of skin biopsies from keloids (KD) and KD neighboring normal control subjects (KN). Following rigorous quality-control protocols, we acquired 60,732 superior-grade cells for additional examination. We first conducted normalization and then applied uniform manifold approximation and projection (UMAP). The cells were grouped into twenty-one clusters, primarily according to their cell types, as annotated based on known cell lineage-specific marker genes unique to T lymphocytes, B lymphocytes, fibroblasts, NK cells, mast cells, myeloid cells, epithelial cells, endothelial cells, oligodendrocytes, melanocytes, and undetermined cells (Fig. 1A). Considering melanocytes are the primary cells responsible for pigmentation, we thus extracted skin melanocytes from the scRNA-seq dataset. As shown in Fig. 1B-C, the pigment signaling critical members *PMEL*, *MITF*, melan-A (*MLANA*), tyrosinase-related protein 1 (*TYRP1*), and dopachrome tautomerase (*DCT*, also known as *TYRP2*) significantly increased in keloid melanocytes. We also evaluated the levels of melanogenesis-related genes in other cell types to detect whether melanin was actually produced explicitly by melanocytes in KD. Results showed that *PMEL*, *MITF*, *MLANA*, *TYR*, *TYRP1*, and *TYRP2* were predominantly expressed in melanocytes (Supplementary Figure S1). Next, a double immunofluorescence assay consistently revealed that melanocytes from KD are more active than normal skin from KN since there are more MITF-positive melanocytes in the epidermal layer of keloid tissue (Fig. 1D-E). The increase of *PMEL*, *MITF*, *MLANA*, *TYRP1*, and *TYRP2* was further validated in keloid skin tissues (Fig. 1F).

Next, the Kyoto Encyclopedia of Genes and Genomes (KEGG) analysis was applied to identify pathways that were significantly enriched in melanocytes of keloid compared with that of adjacent normal skins. We thus found that pigment granule, melanosome signaling, and pigmentation signaling were significantly enriched in keloid melanocytes (Fig. 1G). Masson-Fontana staining further revealed a thickened epidermis (Fig. 1H) and increased melanin in the epidermis as quantified by the positive Masson-Fontana staining (Fig. 1I-J), consistent with the results shown in Fig. 1K that elevated melanin content in keloid skin homogenate by spectrophotometric measurement of melanin at 490 nm of absorbance. Furthermore, a significant correlation was found between melanin contents and the Keloid Area and Severity Index (KASI), a clinical index used to assess the severity of keloid (Fig. 1L). Besides, we found that the KD skin color was significantly darker than the KN skin (Fig. 1M). More interestingly, we found that the skin color at the lesion site gradually became lighter as we recovered from the surgery (Fig. 1N).

Together, these results suggest that the melanin metabolism in keloid is disrupted and may be associated with keloid onset, severity, and prognosis.

Melanin secreted by melanocytes of KD is one of the important factors to activate Melanocytes-induced fibroblasts

We evaluated the histopathology of keloid by Hematoxylin-Eosin (HE) and Masson's trichrome staining (Masson's) staining and found a thickened dermis and increased collagen contents in the keloid skin tissues compared with normal skin tissues (Fig. 2A-C). S100A4, also known as fibroblast-specific protein-1 (FSP1), is a typical marker for skin fibroblasts. Moreover, S100A4 expression is significantly higher during fibroblast proliferation or activation and represents more severe fibrotic lesions [36, 37]. Fluorescent immunohistochemistry staining revealed the accumulation of S100A4-positive areas in keloid skin tissues (Fig. 2D). These results suggested that the hyperactivation of fibroblasts and

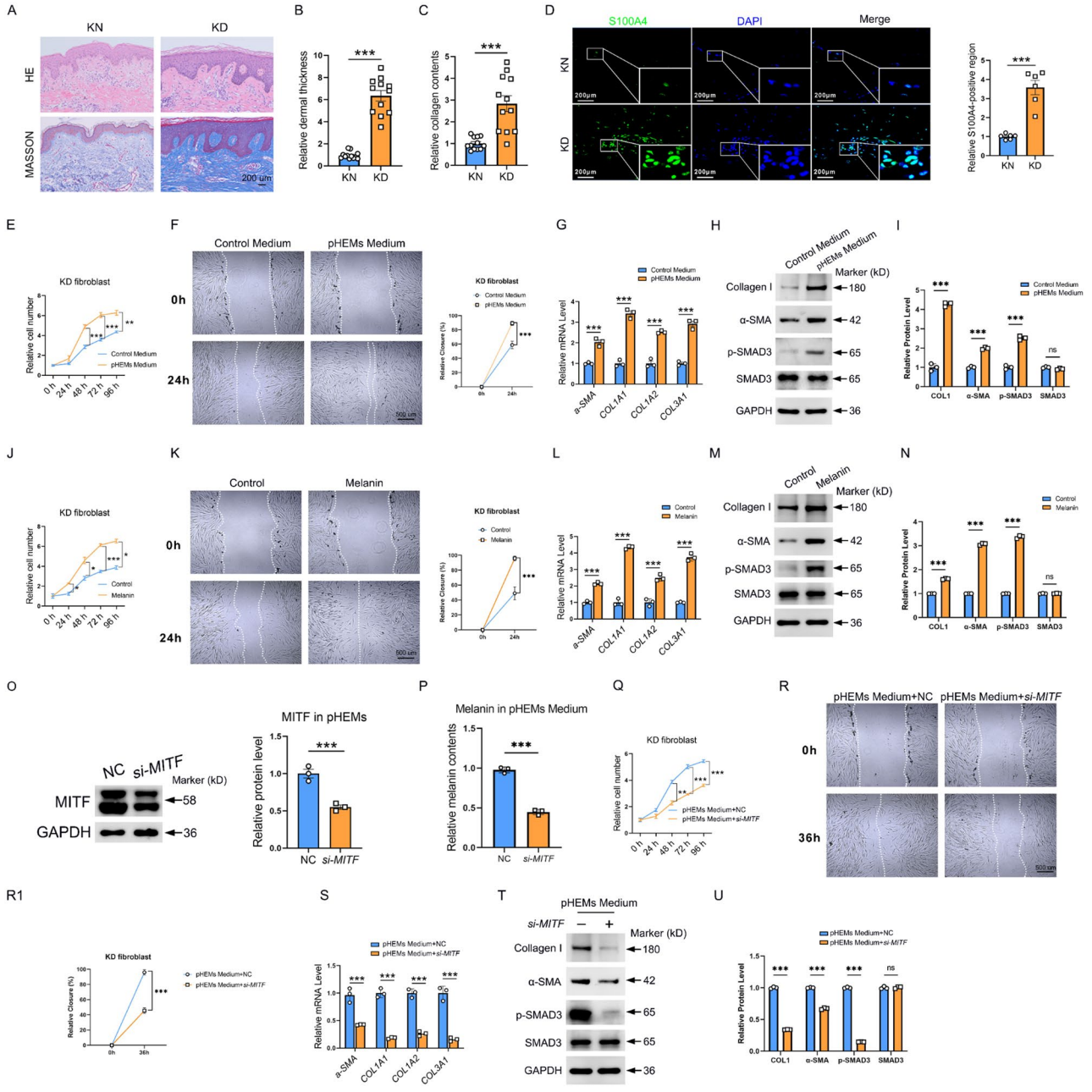

Fig. 2 Melanin from melanocytes promotes fibroblast growth, migration, and collagen deposition. (**A**) HE and Masson's staining of KN and keloid skin tissues. *N* = 12. Scale bar, 200 μm. (**B-C)** Dermal thickness and collagen content. **(D)** Immunofluorescence assay and cell count of S100A4-positive fibroblast cells in keloid skin tissues. *N* = 6. Scale bar: 50 μm. (**E-F**) Cell growth and migration of KD fibroblast cells with or without pHEMs medium treatment. (**G-I**) qPCR and western blot detection of fibrosis-related proteins in KD fibroblast cells with or without pHEMs medium treatment. (**J-K**) Cell growth and migration of KD fibroblast cells with or without melanin treatment. (**L-N**) qPCR and western blot detection of fibrosis-related proteins in KD fibroblast cells with or without melanin treatment. (**O**) Western blot detection of MITF in pHEMs with NC siRNA or *si-MITF*. (**P**) Quantifying isolated melanin from pHEMs medium by spectrophotometric measurement at 490 nm of absorbance. (**Q**) Cell growth of KD fibroblast cells pretreated with NC-transfected pHEMs medium (pHEMs Medium + NC) or *si-MITF*-transfected pHEMs medium (pHEMs Medium + *si-MITF*). (**R-R1**) Cell migration of KD fibroblast cells pretreated with pHEMs medium with NC siRNA or *si-MITF*. (**S-U**) qPCR and western blot detection of fibrosis-related proteins in KD fibroblast cells treated with pHEMs Medium + NC or pHEMs Medium + *si-MITF*. The Scale bar in data F, K, and R were 50 μm. The experiments in E-U were repeated three times independently. **P* < 0.05; ***P* < 0.001; ****P* < 0.001

collagen deposition are apparent characteristics of keloid. Next, we collected the supernatants from primary human epidermal melanocytes (pHEMs) after 48 h of culture (pHEMs Medium) and added them into fibroblast cells. The control medium is a fresh medium without pHEMs culture. Cell counting and wounding healing results showed that the pHEMs Medium significantly stimulated the proliferation and migration of fibroblasts (Fig. 2E-F). qPCR analysis showed that fibrosis-related genes *a-SMA*, *COL1A1*, *COL1A2*, and *COL3A1* were significantly increased (Fig. 2G). TGF-β/p-SMAD3 signaling is a critical pathway in fibroblast activation, proliferation, and migration [36]. Western blot further confirmed that cultured melanocyte supernatants significantly increased fibrosis-related protein expression and p-SMAD3 levels in fibroblast cells (Fig. 2H-I).

As we thus found that pigmentation signaling significantly increased in keloid melanocytes, we, therefore, detected whether melanin has the effect of activating fibroblasts. We then added melanin to the fibroblasts and found that melanin significantly stimulated the proliferation and migration of the fibroblasts (Fig. 2J-K). qPCR and Western blot further revealed that melanin significantly upregulated the expression of fibrosis-related proteins *a-SMA*, *COL1A1*, *COL1A2*, *and COL3A1* (Fig. 2L-N). In addition, we knocked down the critical protein of melanin synthesis MITF in pHEMs, and the cell supernatant was collected after 48 h to make pHEMs Medium + NC and pHEMs Medium + *si-MITF*, respectively. The results showed that melanin levels in the pHEMs supernatant were significantly decreased after *si-MITF* treatment. Moreover, the cell proliferation, migration, and profibrotic effect on fibroblasts of pHEMs significantly reduced after MITF knockdown (Fig. 2O-U).

Since MITF is known to be required for melanin synthesis, we next analyze its expression levels in fibroblasts cultured or not in pHEMs or in the presence of melanin. We detected the levels of MITF in fibroblasts and found that the endogenous MITF levels in fibroblast cells were relatively weak. In addition, the expression of MITF in fibroblasts was not significantly altered by adding melanin or pHEMs culture medium (Supplementary Figure S2). These results suggest that melanocytes deliver the melanin accumulated in fibroblasts and are not synthesized by the fibroblast cells themselves. A critical question is how fibroblasts uptake extracellular melanin. F2R-like trypsin receptor 1 (F2RL1, also known as PAR-2) is an essential receptor for skin pigmentation that stimulates the uptake of melanosomes [38]. We next found an increase of PAR-2 in KD fibroblasts, especially in CCL19- and CTHRC1-positive fibroblasts, by scRNA-seq analysis (Supplementary Figure S3A-B).

In conclusion, melanocytes in KD promote fibroblasts' proliferation, migration, and fibrosis, at least by over-synthesizing melanin.

Melanin impairs the basal membranes to facilitate its transfer to the dermis in KD

An intriguing question is whether melanin could transfer to the dermal layers in KD, and the mechanism and specific compartments involved in this process remain to be elucidated. We further tested the location of melanin in the skin by Masson-Fontana staining and found that melanin is present in the papillary dermis of KD but not in the KN dermis (Fig. 3A). The elevated isolated melanin contents in the dermis of the keloid were also validated (Fig. 3B). We examined the integrity of the basal layer since it acts as a barrier between the epidermis and dermis. We first analyzed the DEGs in basal cells and found that the pathways involved in IL-17, TNF-α, cytokine-cytokine receptor interaction, chemokine, and tight junction were widely altered in KD basal cells (Fig. 3C-D). Moreover, the genes *CCL2*, *JUN*, *FOS*, *TNFSF10*, *S100A9*, and *S100A8* involved in inflammation were significantly upregulated (Fig. 3E). In contrast, the levels of *NFKBIA*, whose deficiency aggravates inflammation, were lower in KD basal cells. Besides, the genes *CLDN1*, *ACTG1*, and *ACTN4*, involved in tight junction, were significantly downregulated (Fig. 3E). qPCR analysis revealed increased inflammatory genes and decreased tight junction-related genes in KD (Fig. 3F). ELISA analysis further revealed that CCL2 and S100A8/A9 were higher in KD than in KN skins (Fig. 3G).

Additionally, scRNA-seq revealed the basal layer markers *KRT15* and the hemidesmosome components of basal cells collagen XVII (*COL17A1*) become downregulated in the KD skin basal layer and then validated by qPCR (Fig. 3E **and H**). IHC analysis further confirmed reduced COL17A1 in the KD epidermis (Fig. 3I). Next, we found a significantly decreased COL17A1 protein in KD compared with KN skin tissue (Fig. 3J).

Ex vivo skin explants and in vitro cell experiments were performed to address whether impaired basal membrane in KD is associated with excessive melanin. As shown in Fig. 3K, melanin was added to cultured KD skin explants. qPCR and ELISA consistently demonstrated melanin-induced significant inflammation in skin explants (Fig. 3L-M). In contrast, melanin significantly downregulated COL17A1 expression at mRNA and protein levels (Fig. 3N-O). To further confirm the ability of melanin to induce increased inflammation and permeability in skin basal cells, in vitro cultured human skin basal cells TE 354.T was used for further experiments. It was found that melanin significantly promoted the secretion of inflammatory factors in TE 354.T cells, including significantly increased expression of CCL2, S100A8/A9 (Fig. 3P).

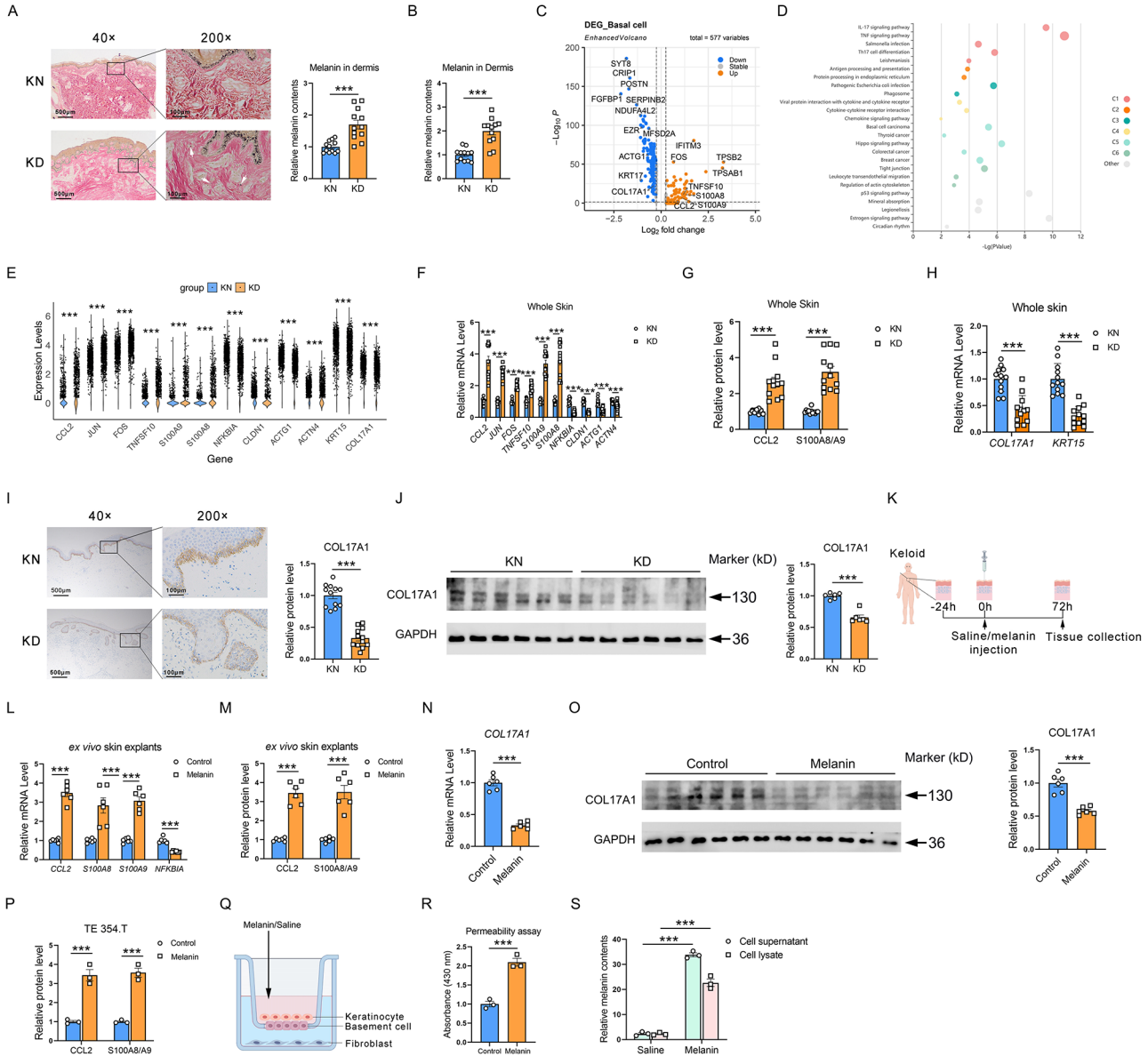

Fig. 3 Melanin transfers to the skin dermis by disrupting the basal membrane. (**A**) Masson-Fontana staining and quantification of melanin contents in the skin dermis. *N* = 12. The 40× scale bar is 500 μm and the 200× scale bar is 100 μm, respectively. (**B**) Quantification of the isolated melanin from the separated dermis. *N* = 12. (**C**) The Volcano map of DEGs between KN and KD basal cells. (**D**) GO and KEGG orthologs of the DEGs in basal cells. (**E**) Violin plots represent the expression of inflammation, tight junction, and basal marker genes in basal cells from KN and KD skins. (**F**) qPCR analysis of inflammation and tight junction genes in KN and KD skins. *N* = 12. (**G**) ELISA analysis of CCL2 and S100A8/A9 in KN and KD skins. *N* = 12. (**H**) qPCR analysis of *COL17A1* and *KRT15* in KN and KD skins. *N* = 12. (**I**) Immunohistochemistry of COL17A1 on skin sections from the KN and KD. *N* = 12. (**J**) Protein expression of COL17A1 in KN and KD skins. (**K**) The schematic diagram of ex vivo explants culture and intraepidermal melanin injection. (**L**) qPCR analysis of inflammation genes after melanin treatment in skin explants. (**M**) ELISA analysis of CCL2 and S100A8/A9 after melanin treatment in skin explants. (**N-O**) mRNA and protein levels of COL17A1 in skin explants after melanin treatment. (**P**) CCL2 and S100A8/A9 protein expression in TE 354.T basal cells. (**Q**) The schematic diagram of co-culture of keratinocytes, basal cells, and fibroblasts. (**R**) Cell permeability assay. (**S**) Melanin content in cell medium and fibroblast cells with or without melanin treatment. The experiments in P-S were repeated three times independently. **P* < 0.05; ***P* < 0.001; ****P* < 0.001

Moreover, the cell permeability assay indicated increased permeability ability with 100 ug/ml of melanin (Fig. 3Q-R). In addition, in the medium outside the chamber and in the fibroblast cell, melanin could be effectively detected (Fig. 3S).

Collectively, these results suggest that the abnormally increased melanin in KD can be transferred to the dermal layer of the skin by inducing inflammation in the basal layer of cells and increasing their permeability.

Melanin activates fibrosis response in fibroblasts by inducing iron overload

To further investigate the mechanisms underlying melanin-induced fibrogenesis of skin fibroblasts, an integrative analysis of differentially expressed genes (DEGs) was performed (|Fold change| > 1, and q-value < 0.05). As shown in Fig. 4A, the heatmap of the gene expression profile was distinct between the negative control (NC) group and

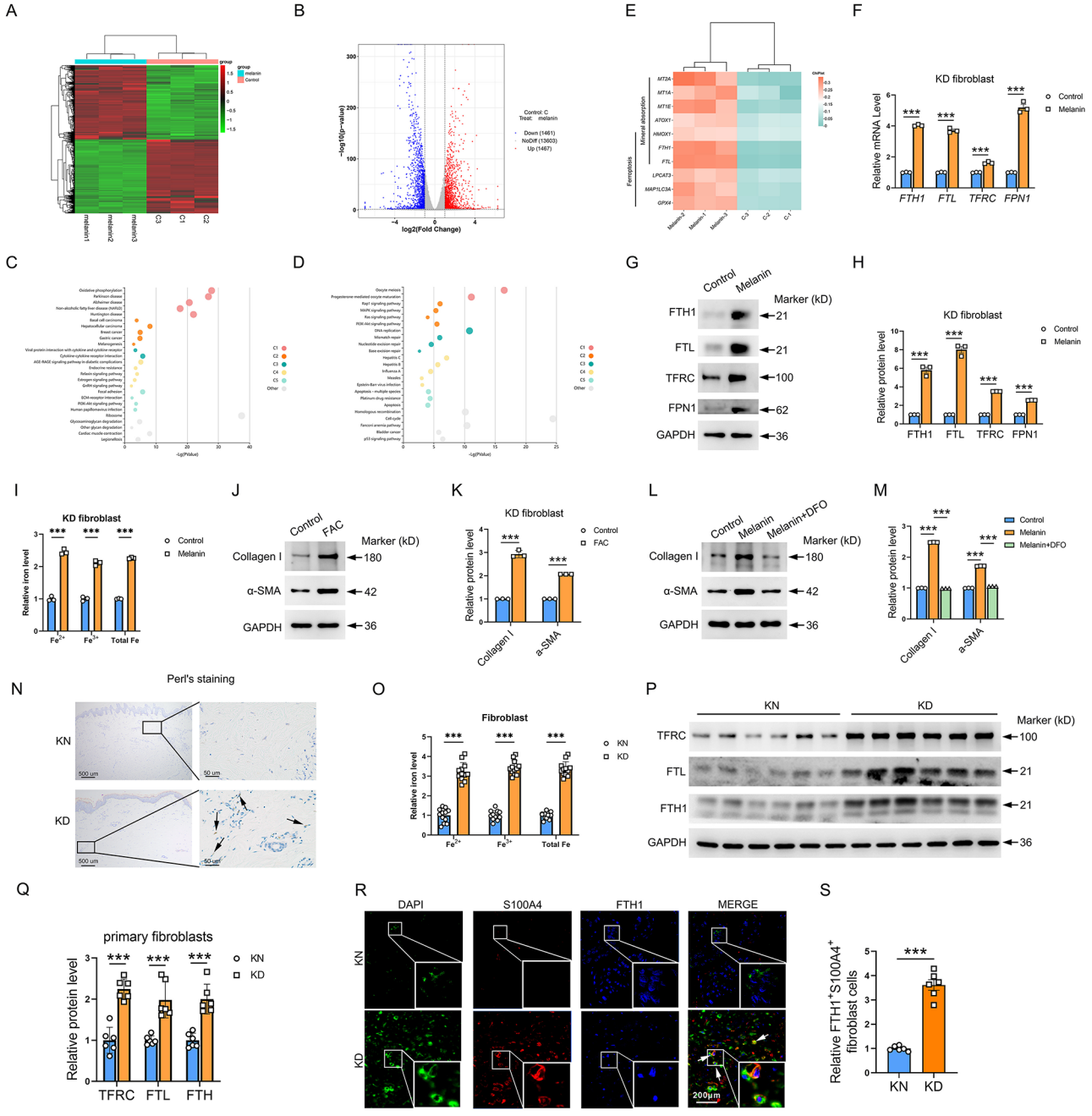

Fig. 4 Melanin induces iron overload to activate fibroblasts. (**A-B**) The heatmap and Volcano map of DEGs between control and 100 ug/ml melanin-treated fibroblasts. (**C-D**) GO and KEGG orthologs of the upregulated and downregulated DEGs. (**E**) The heatmap of the upregulated DEGs involved in mineral absorption and ferroptosis. (**F**) mRNA expression of *FTH1*, *FTL*, *TFRC* and *FPN1* in primary KD fibroblasts. (**G-H**) FTH1, FTL, TFRC, and FPN1 protein expression in primary KD fibroblasts. (**I**) Total iron, Fe^{2+}, and Fe^{3+} levels in melanin-treated KD fibroblasts. (**J-K**) Protein expression of α-SMA and Collagen I in primary KD fibroblasts. (**L-M**) Protein expression of α-SMA and Collagen I in primary KD fibroblasts. (**N**) Perl's staining of skin tissues. Scale bar: 500 μm and 50 μm. (**O**) Total iron, Fe^{2+}, and Fe^{3+} levels in KN and KD fibroblasts. (**P-Q**) Protein expression of FTH1, FTL, and TFRC in primary KD fibroblasts. $N = 6$. (**R-S**) Immunofluorescence assay and cell count of $FTH1^{+}S100A4^{+}$ fibroblast cells in keloid skin tissues. $N = 6$. Scale bar: 200 μm. The experiments in A-M were repeated three times independently. $^{*}P < 0.05$; $^{**}P < 0.001$; $^{***}P < 0.001$

melanin group by RNA-seq assay. Finally, 2,928 DEGs were identified, including 1,461 downregulated and 1,467 upregulated genes (Fig. 4B). Furthermore, GO and KEGG orthologs showed the upregulated DEGs primarily divided into melanogenesis, cytokine-cytokine receptor interaction, focal adhesion, PI3K/AKT, and ECM-receptor pathways (Fig. 4C). These results indicated that the profibrotic effect of melanin was multi-pathway and biology process-dependent. Besides, the downregulated DEGs are primarily divided into apoptosis, cell cycle, and P53 signaling pathways (Fig. 4D). The intriguing mineral absorption pathway, especially the iron metabolism-associated pathway, was significantly enriched in melanin groups, and the detailed genes were shown in Fig. 4E, suggesting abnormal iron metabolism involved in melanin-mediated ECM deposition. Next, qPCR and western blot analysis consistently showed significantly elevated ferritin heavy chain 1 (FTH1), ferritin light chain (FTL), transferrin receptor (TFRC), and solute carrier family 40 member 1 (SLC40A1, also known as FPN1) by melanin (Fig. 4F-H). The iron content detection also found melanin increased iron deposition in fibroblasts (Fig. 4I). Moreover, iron supplements (Ferric citrate, FAC) promoted collagen synthesis and a-SMA expression (Fig. 4J-K). In contrast, Deferoxamine (DFO) is an iron chelator widely used to reduce iron accumulation and deposition, significantly diminishing melanin-induced upregulation of collagen and a-SMA (Fig. 4L-M). These results confirmed that melanin-induced fibrogenesis is essentially iron overload-dependent. To further confirm whether iron overload is involved in the pathogenesis of KD, we examined the expression of genes related to iron metabolism in KD patients. Perl's staining revealed apparent iron overload in KD's skin dermis. (Fig. 4N). The isolated iron content in KD fibroblasts significantly increased compared to KN fibroblasts, including total iron, Fe^{2+}, and Fe^{3+} levels (Fig. 4O). Further, we examined the expression levels of the above iron metabolism genes in primary skin fibroblasts. Compared to normal controls, the results showed significantly increased FTH, FTL, and TFRC in KD fibroblasts (Fig. 4P-Q). Besides, FTH1 is a vital indicator protein for intracellular iron content [39], so we examined the expression level of FTH1 in S100A4-positive fibroblasts using a double-immunofluorescence assay. Results showed an increase of $S100A4^{+}FTH1^{+}$ fibroblast cells from KD skin tissues compared to KN (Fig. 4R-S). These results consistently indicate that iron metabolism disorders and iron overload are involved in KD processes.

Collectively, we found that melanin activates the fibroblast fibrotic response by inducing iron overload and ultimately exacerbates the development of KD.

Melanin imparts ferroptosis resistance to fibroblasts

Iron overload is one of the critical causes of ferroptosis. Indeed, melanin significantly upregulated genes involved in ferroptosis, as shown in Fig. 4E. Thus, we examined ferroptosis in fibroblasts treated with melanin. The results showed that contrary to expectations, melanin significantly upregulated the expression of three critical ferroptosis inhibitory factors: glutathione peroxidase 4 (GPX4), solute carrier family 3 member 2 (SLC3A2), and solute carrier family 7 member 11 (SLC7A11), while down-regulated the expression of ferroptosis promoting factors acyl-CoA synthetase long-chain family member 4 (ACSL4) (Fig. 5A-C). Our scRNA-seq results consistently showed a decreased ACSL4 with increased SLC3A2 and GPX4 in KD fibroblasts (Fig. 5D). The LipidROS assay also found that melanin decreased the LipidROS production at baseline and RSL-3-induced conditions in KD fibroblasts (Fig. 5E). Cell Counting assay found that melanin significantly inhibited the decline in fibroblast viability caused by the ferroptosis inducer RSL-3 (a GPX4 inhibitor) (Fig. 5F). Meanwhile, melanin also considerably reduced the content of 4-Hydroxynonenal (4-HNE) and Malondialdehyde (MDA) (Fig. 5G-H). These results suggest that melanin activates the antioxidant signaling pathway of fibroblasts, thereby acquiring ferroptosis resistance. Similarly, to further confirm whether ferroptosis resistance is involved in the pathogenesis of KD, we examined the expression of ferroptosis-related genes in KD. The results showed significantly increased GPX4, SLC3A2, and SLC7A11 in KD fibroblasts compared with healthy control skin tissue fibroblasts (Fig. 5I-J). We next performed an immunofluorescence assay and found an accumulation of GPX4 in S100A4-positive fibroblast cells from keloid skin tissues (Fig. 5K-L).

These results consistently indicate that fibroblast ferroptosis resistance is involved in the KD process.

Melanin induces iron overload and ferroptosis resistance of melanocytes in an autocrine manner and promotes melanin transport to keratinocytes

We have found that melanin secreted by melanocytes can activate fibroblasts through iron overload and ferroptosis resistance, so what effect does melanin have on melanocytes? The qPCR and western detection showed that melanin upregulated the expression of iron metabolism-related genes such as FTH/FTL/TFRC/SLC40A1 in pHEMs (Fig. 6A-C). The iron content test showed that iron ions increased significantly after melanin treatment (Fig. 6D). These results suggest that melanin induces iron overload in melanocytes. Further, cell counting experiments revealed that melanin promotes pHEMs viability and effectively blocks ferroptosis caused by RSL-3 (Fig. 6E). Correspondingly, melanin significantly increased ferroptosis resistance-related proteins GPX4

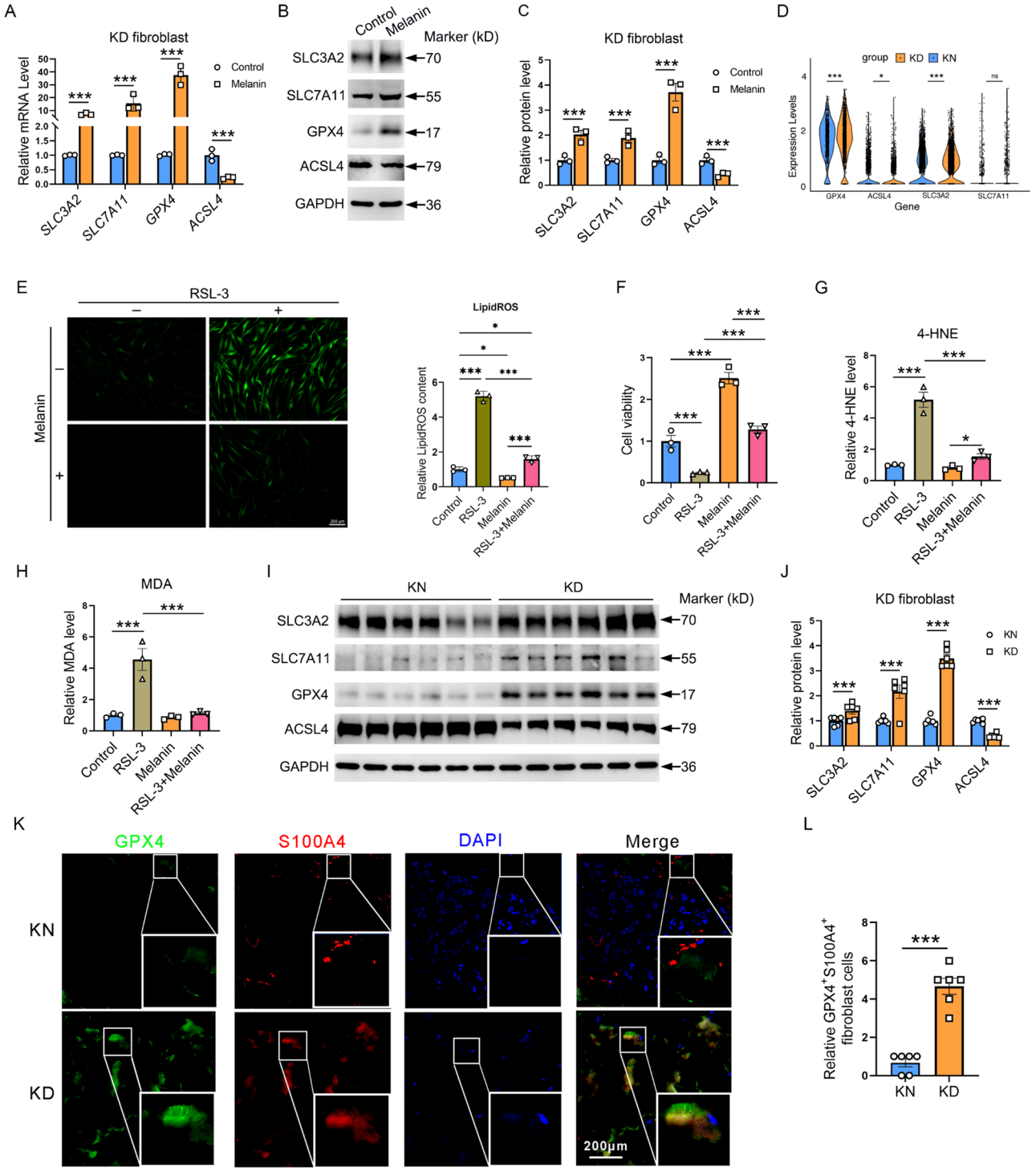

Fig. 5 Melanin inhibits ferroptosis in KD fibroblasts. (**A-C**) qPCR and western blot detection of ferroptosis-inhibitory proteins SLC3A2/SLC7A11/GPX4 and pro-ferroptotic proteins in KD fibroblast cells with or without melanin stimulation. (**D**) The mRNA levels of *ACSL4*, *SLC7A11*, *GPX4*, and *SLC3A2* in KD and KN skin tissues by scRNA-seq analysis. (**E**) Evaluation of the effects of melanin on RSL-3-induced LipidROS in KD fibroblast cells. Scale bar: 200 μm. (**F**) Cell viability of fibroblast cells treated with RSL-3 and melanin by CCK8 assay. (**G-H**) Relative 4-HNE and MDA levels after fibroblast cell treated withRSL-3 and melanin. (**I-J**) Western blot analysis of SLC3A2, SLC7A11, GPX4, and ACSL4 protein levels in KN and KD primary fibroblasts. $N=6$. **(K-L)** Immunofluorescence assay and cell count of $GPX4^{+}S100A4^{+}$ fibroblast cells in keloid skin tissues. $N=6$. Scale bar: 200 μm. The experiments in A-H were repeated three times independently. $^{*}P<0.05$; $^{**}P<0.001$; $^{***}P<0.001$

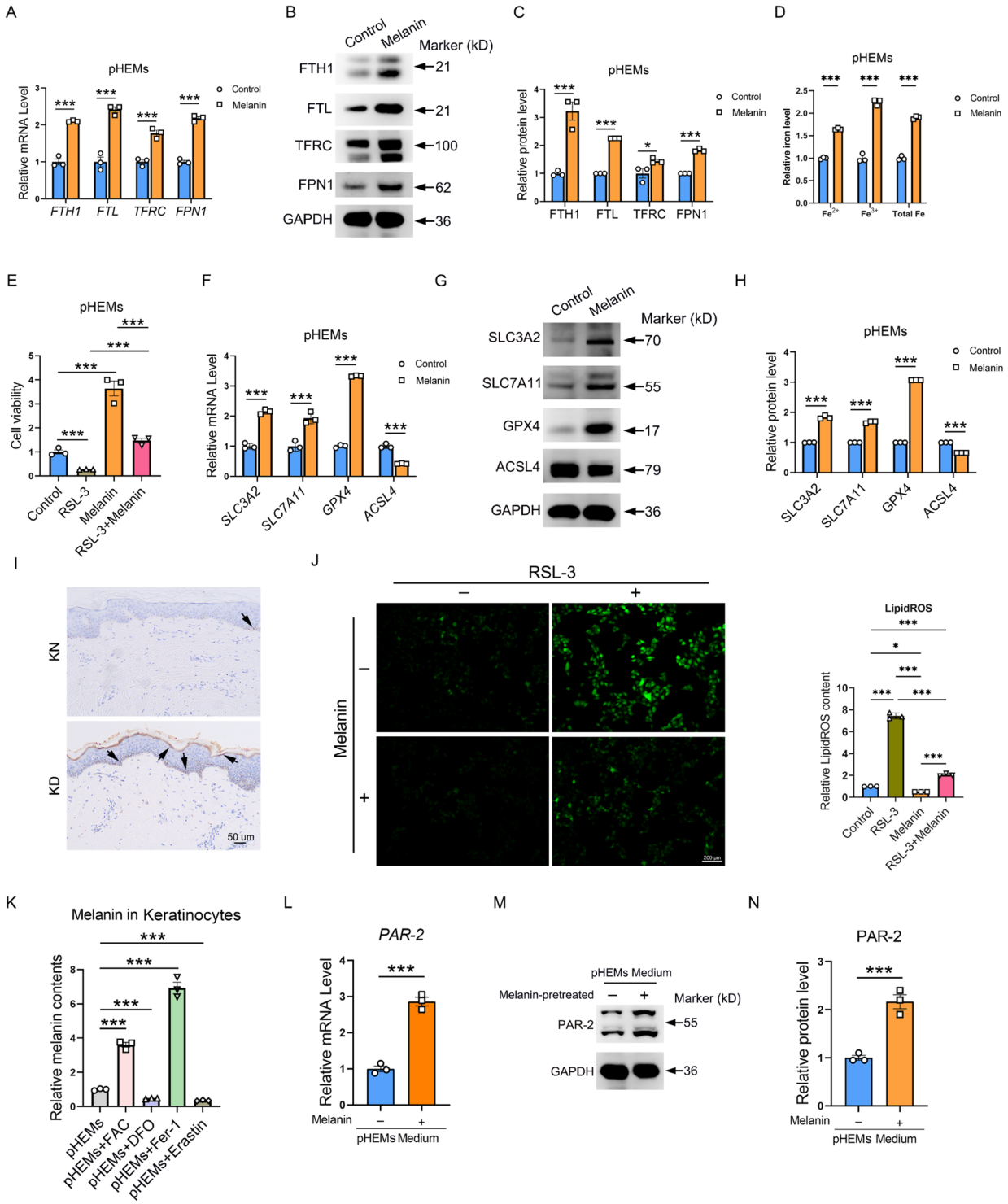

Fig. 6 Melanin-induced iron overload and ferroptosis-resistance in melanocytes and benefited keratinocyte cells absorbing melanin. (**A-C**) The expression of iron metabolism-related genes after 100 ug/ml melanin incubation in pHEMs. (**D**) Total iron, Fe^{2+}, and Fe^{3+} levels in melanin-treated melanocytes. (**E**) Cell viability of pHEMs treated with RSL-3 and melanin by CCK8 assay. **(F-H)** qPCR and western blot detection of ferroptosis-inhibitory proteins SLC3A2/SLC7A11/GPX4 and pro-ferroptotic proteins in pHEMs with or without melanin stimulation. (**I**) Perl's staining of iron content in epidermal skin tissues. Scale bar: 50 μm. (**J**) Evaluation of the effects of melanin on RSL-3-induced LipidROS in pHEMs. Scale bar: 200 μm. (**K**) Melanin contents in HaCaT cells. (**L-N**) qPCR and western blot analysis of PAR-2 protein levels in HaCaT cells. The experiments were repeated three times independently. *$P < 0.05$; **$P < 0.001$; ***$P < 0.001$

and System X_C^- (SLC3A2/SLC7A11) while substantially decreasing ACSL4 (Fig. 6F-H). Moreover, the Perl's showed increased iron deposition in KD keratinocytes, and the LipidROS assay revealed that melanin reduced the production of LipidROS at baseline and RSL-3-induced conditions in keratinocytes (Fig. 6I-J). These results strongly suggest that melanin can also cause iron overload and ferroptosis resistance in melanocytes in an autocrine manner.

Melanin synthesized by melanocytes will transport to keratinocytes, and only under stimulation, such as ultraviolet light, will they show different skin tones. Therefore, we further constructed the co-culture system of melanocytes and keratinocytes. The Transwell experiment found that pHEMs with FAC or Ferrostatin-1 (Fer-1) treatment significantly increased melanin content in keratinocyte HaCaT cells compared to the pHEMs without FAC or Fer-1 treatment. In addition, pHEMs with DFO and Erastin (an inducer of ferroptosis) treatment significantly reduced melanin in HaCaT cells, respectively (Fig. 6K). Erastin is known to bind Voltage Dependent Anion Channel 2/3 (VDAC2/3). We next examined the altered mitochondrial function of Erastin-treated pHEMs and found that Erastin increased mitochondrial membrane potential (MMP) and mitochondrial ROS levels in pHEMs, suggesting mitochondrial dysfunction may be involved in Erastin-mediated melanin transfer from melanocyte to keratinocyte (Supplementary Figure S4A and B). qPCR and western experiments showed that pHEMs supernatants with melanin incubation caused significant upregulation of PAR-2 in HaCaT cells compared to the control pHEMs culture supernatant (Fig. 6L-N).

These results suggest that ferroptosis resistance contributes to melanin-to-keratinocyte transport in melanocytes.

Inhibition of melanin synthesis alleviates KD in nude mice

Given the promotion of melanin on proliferation, cell migration, and collagen deposition in dermal fibroblasts, we investigated the possibility of inhibiting melanogenesis to alleviate keloid in vivo. The keloid-bearing mouse received repeated saline or melanogenesis inhibitor 5 mg/kg ML329 injections once every three days and harvested the grafts on day 21 (Fig. 7A). Subcutaneous keloid grafts were morphologically smaller in volume and weight than the NC group (Fig. 7B-D). Histologically, ML329 treatment reduced the density of dermal tissue (Fig. 7E). Sircol assay showed the release of collagen fiber bundles and the downregulation of collagen content (Fig. 7F). We also detected melanin contents in these grafts and found a decrease in keloid grafts after ML329 treatment (Fig. 7G). Furthermore, ML329 decreased iron levels (Fig. 7H) while increasing MDA levels (Fig. 7I). An immunofluorescence assay consistently revealed that ML329 reduced ferritin and GPX4 in the keloid fibroblast, suggesting released iron overload and ferroptosis resistance (Fig. 7J-M). These results demonstrated that melanogenesis inhibition could alleviate keloid progression by decreasing melanogenesis activities, iron overload, and ferroptosis in vivo.

As reported, using an MITF inhibitor in humans could cause side effects, such as inducing vitiligo and affecting mast cells and bone regeneration. To further evaluate the safety of ML329 in treating keloids, we examined inflammation and melanin changes in KN and KD skin explants treated with ML329. Our findings indicate that ML329 does not inhibit melanin production in normal skin (KN), but it significantly suppresses the synthesis of KD melanin in cultured ex vivo skin explants (Supplementary Figure S5A). Interestingly, ML329 appears to restore melanin levels to those typical of KN rather than causing further reduction. The emerging role of MITF as a critical regulator of immunity has been highlighted [40]. We investigated the expression of mast cell marker proto-oncogene, receptor tyrosine kinase (c-Kit, also known as CD117), and cytokines secreted by mast cells, including IL-4 and TNF-α, in skin explants following ML329 treatment and discovered that ML329 can also restore these proteins to near physiological states (Supplementary Figure S5B). ML329 is more likely to revert abnormally elevated melanin and inflammation to normal levels, thereby promoting skin homeostasis. Since keloid tissue grows outwardly, the skin dermis is distanced from the skeleton. Therefore, we may mitigate the side effects through topical application or epidermal medication to avoid unexpected side effects on osteogenesis and osteoclast cells. In conclusion, the appropriate concentration and medication regimen to restore the homeostasis of skin melanin metabolism and immune response will be beneficial in reducing side effects.

Discussion

Keloid is a fibrotic skin disease characterized by collagen deposition, prolonged inflammation, and pain or itching [2]. The pathogenesis of KD is complex and unclear and, therefore, lacks an effective clinical target. A large body of evidence suggests that the formation of KD is a complex multicellular process. Notably, fibroblasts, the primary effector cells of fibrogenesis in KD, undergo a wide range of abnormal processes during KD formation, such as proliferation, migration, activation, and collagen deposition. However, the causative factors leading to fibroblast abnormalities, especially the abnormal regulatory mechanisms between cellular communication, are not apparent. Therefore, it is crucial to visualize the aberrant communication between various types of cells in KD skin tissues to elucidate the mechanisms of fibrosis and develop feasible KD targets.

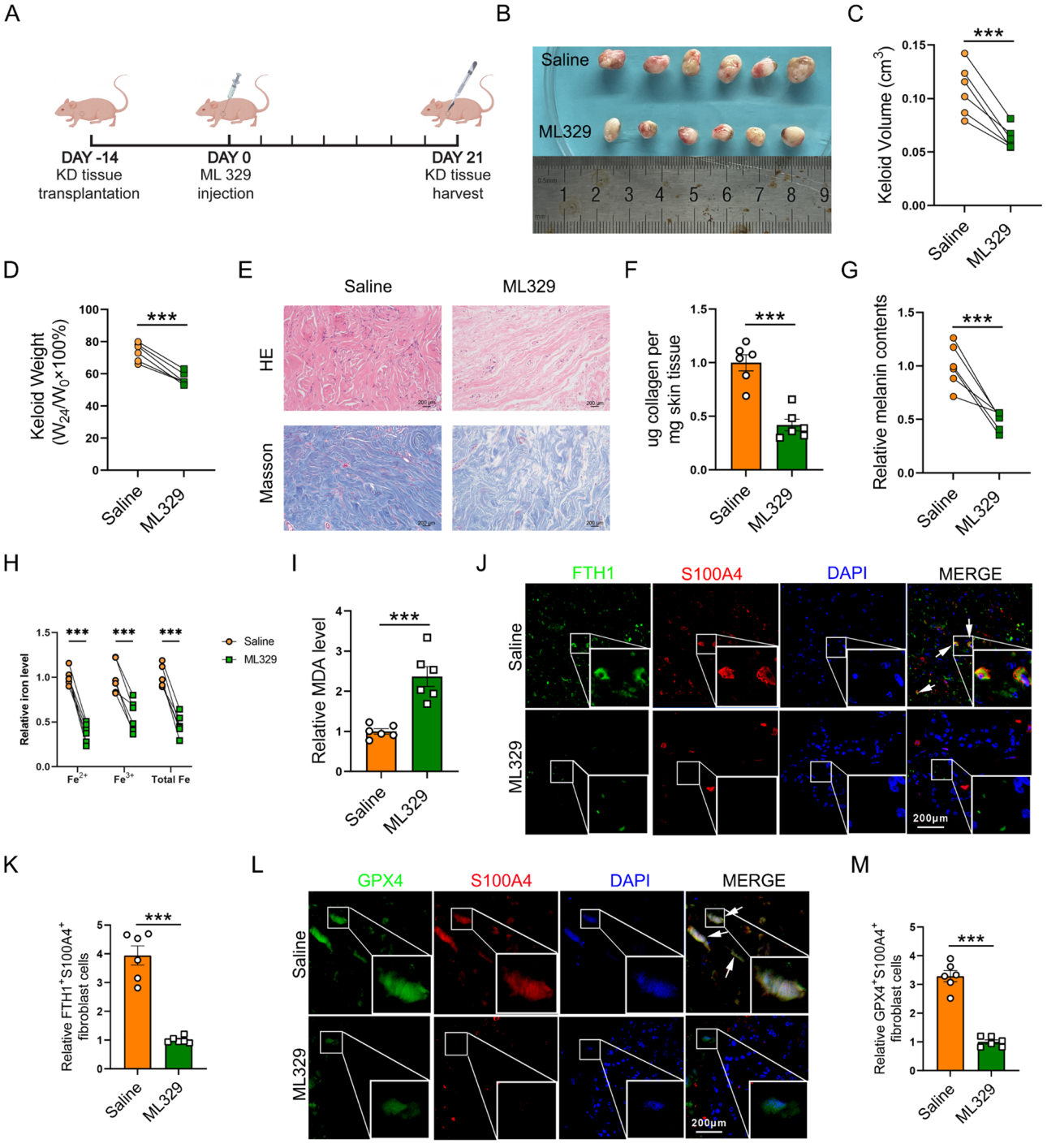

Fig. 7 ML329 improved skin fibrosis in vivo. (**A**) The keloid-bearing mouse model construction and subcutaneous ML329 injection. (**B**) Grafts were collected on day 21 and separated into saline and ML329 groups. (**C-D**) Volume and weight measurement of grafts. (**E**) HE and Masson stain the collected grafts. Scale bar, 200 μm. (**F**) Sircol assay showed a decrease in ECM in the ML329 groups. (**G-I**) Measurements of melanin, total iron, Fe^{2+}, Fe^{3+} levels, and MDA levels in KD grafts. (**J-M**) Immunofluorescence assay of $FTH1^{+}S100A4^{+}$ fibroblast cells and $GPX4^{+}S100A4^{+}$ fibroblast cells. Scale bar, 200 μm. $N=6$. $^{*}P<0.05$; $^{**}P<0.001$; $^{***}P<0.001$

Through the analysis of our KD single-cell data, we found a significantly enriched pigmentation signaling pathway of melanocytes in KD tissue, and the detection of Masson-Fontana staining and isolated melanin content measurement further confirmed the excessive activation of melanin synthesis in KD melanocytes. Previous studies have also confirmed our findings and supported the theory of melanin metabolism disorder in the formation

of KD [22]. Notably, to avoid the difference in melanin content caused by different KD sites, we obtained the control skin tissues used to detect melanin content in this study from KD-adjacent tissues. Indeed, these melanogenesis-related genes are also expressed in other organs (The Human Protein Atlas, https://www.proteinatlas.org/), such as the retina, where melanin is produced by retinal pigment epithelium [41]. In the brain, the neuromelanin may be produced by neuron cells [42]. Melanocytes can produce black eumelanin and yellow phaeomelanin. In our study, the melanin content was measured by Masson-Fontana staining, or the cell pellets were dissolved in NaOH, and the absorbance was detected at 490 nm. These methods are relatively specific methods to detect melanin, as in a previous study [32]. Further, we found that melanocyte medium significantly promoted the proliferation, migration, and collagen deposition of fibroblasts, strengthening the critical role of melanocytes in KD fibrosis. Since we found enhanced melanin synthesis in KD melanocytes, we suspect melanin may be involved in fibroblast overactivation. The results showed that melanin can significantly promote the above fibroblast dysfunction. Knockdown of MITF, the vital factor of melanin anabolic metabolism, can substantially reduce melanin content and attenuate the promotional role of melanocytes on fibroblast cell activation. Previous studies have reported that melanocytes can activate KD fibroblasts through exosomal microRNA [22], and our findings further enrich our understanding of KD pathogenesis from the perspective of melanin anabolic abnormalities.

To explore the mechanism of melanin-activated fibroblasts, we found that melanin can lead to the up-regulation of several essential iron metabolic genes, such as Ferritin, TFRC, and SLC40A1, accompanied by apparent iron overload. DFO-chelated iron significantly inhibited melanin-induced collagen deposition, suggesting that melanin-induced fibroblast activation was iron overload dependent. Although iron overload is prone to ferroptosis, we found that melanin-treated fibroblasts have a strong capacity for ROS clearance, thus offsetting the risk of ferroptosis from iron overload and ultimately displaying ferroptosis resistance. In addition, iron overload, ferroptosis resistance, and related metabolic gene abnormalities were also verified in keloid tissue and primary fibroblasts, further suggesting that iron metabolism and ferroptosis abnormalities are closely associated with melanin metabolism abnormalities [43] and participate in the pathogenesis of KD [44, 45]. During KD, fibroblasts benefit from functional activation induced by iron overload caused by melanin on the one hand, and from the ability to resist ferroptosis caused by melanin to gain immortality, which can at least partially explain why the dermal cortex is massively thickened and fibrotic in KD. The question of whether melanin could transfer to the dermal layers in KD is not only intriguing but also of significant importance. The mechanism and specific compartments involved in this process, which we are yet to understand fully, could hold the key to unlocking new treatments and preventive measures. Our findings revealed that excessive inflammation and increased permeability of basal cells in KD contribute to the melanin transfer to fibroblast cells. The promotional effect of melanin on inflammation was also supported by a previous study [46]. Interestingly, scRNA-seq analysis revealed that fibroblasts also expressed a low level of PAR-2 and increased in KD fibroblasts, especially in CCL19- and CTHRC1-positive fibroblasts. CTHRC1-positive fibroblasts are potent profibrotic fibroblast subpopulations, while CCL19-positive fibroblasts are potent proinflammatory fibroblast subpopulations. We speculated that melanin may also be involved in persistent inflammation in KD. Moreover, these findings have significant implications for our understanding of KD based on the opinion of crosstalk between the epidermis and dermis and could potentially lead to the development of new therapeutic strategies. Therefore, the mechanism of melanin transfer to the dermis in KD is at least related to the damage of the basal layer and enhanced melanin receptor levels in dermal fibroblasts. In addition to fibroblasts, we found that melanin can also act on melanocytes in an autocrine form and cause melanocyte ferroptosis resistance. In the co-culture system of melanocytes and keratinocytes, compared with the control group, melanocytes with ferroptosis resistance may enhance the expression of PAR-2 in keratinocytes, forcing them to absorb more melanin. Therefore, we concluded that the abnormal melanin metabolism in KD involves various cell types. Melanin-mediated aberrant communication between epidermal cells, melanocytes, basement membrane cells, and fibroblasts may be a novel mechanism in the pathogenesis of KD. To this end, we examined the mutual ability of these types of cells in KN and KD and found that the mutual communication between these four types of cells was significantly higher in KD than in KN (Supplementary Figure S6). Melanocytes are located in the basal layer of the skin and secrete a large amount of melanin, which is transported to the subcutaneous dermis to activate fibroblasts and cause fibrosis. Transport upward to the stratum corneum, causing darkening of the skin [47]. The incidence of KD in dark-skinned people is much higher than that in light-skinned people [48]. Our study reveals the role and mechanism of the abnormal axis of melanin synthesis, iron metabolism, and ferroptosis in KD. Our study also has good clinical significance, especially for individuals with dark skin color, who should pay more attention to iron metabolism levels to prevent and treat KD effectively. Indeed, melanocytes existed in the skin tissue and the uvea (the pigment layer behind the iris) of

the eye [41], suggesting that regulating iron metabolism may also contribute to eye diseases due to abnormal melanin metabolism. In addition, skin iron overload can also affect the skin's color depth [21, 49]. Therefore, the effect of iron overload on skin color should also be considered while reducing melanin deposition in the whitening field. Inhibiting iron overload while inhibiting melanin may achieve a better whitening effect. Similarly, the darker skin color of KD patients is related to excessive melanin on the one hand, and iron deposits caused by black, on the other hand, further deepen the skin color. In vivo, we further demonstrated that ML329 can reduce the melanin synthesis of keloid-bearing mice. In addition, ML329, an MITF inhibitor, which effectively restores the sensitivity to palbociclib in CDK4/6i-resistant cancer cells [50], significantly inhibited iron overload and ferroptosis resistance. More importantly, ML329 inhibited KD collagen synthesis and improved keloid morphology and histology.

Interestingly, our findings from the melanin study will contribute to a better understanding of the significant variations in keloid and melanoma incidence among different races. The deficiency of adequate melanin protection makes light-skinned individuals in White more susceptible to melanoma when exposed to ultraviolet rays and other harmful stimuli. Recent research has demonstrated that restoring melanin synthesis capacity can notably decrease melanoma metastasis [51]. Conversely, dark-skinned individuals such as Asians benefit from the high levels of protective melanin, which reduces their risk of developing melanoma by shielding skin cells from UV damage. However, due to robust melanin synthesis, fibroblasts deep within the dermis are activated, increasing susceptibility to keloids. Importantly, we have identified ML329 as a promising inhibitor of MITF, offering the potential for balanced regulation of melanin metabolism that could significantly contribute to clinical practices aimed at preventing and controlling both keloid formation and melanoma. Collectively, we report that an increase in melanin in keloid is associated with an increase in iron overload, ferroptosis resistance, and collagen deposition in keloid dermal fibroblasts. The inhibition of melanin-associated cells and pathways may provide new insight into keloid therapy.

This study reveals abnormally elevated melanin in keloid patients induces aberrant keratinocyte-melanocyte-basal-fibroblast cell communication and promotes fibroblast collagen production. However, our study still has some limitations that need to be addressed in future work. First, this pathogenesis may be more applicable to dark-skinned individuals. For those lighter-skinned white people, melanin itself is lower, so whether melanin is elevated in white keloid processes and the extent to which melanin contributes to the pathogenesis of white keloid remains to be investigated. Second, although we found that dermal fibroblasts can take up melanin, how melanocytes deliver melanin, how fibroblasts take up melanin, and the specific molecular mechanisms involved in this delivery process are unclear. The solution to this problem will also help to analyze the mechanism of other dermal melanin deposition diseases, such as melasma and melioidosis. Third, we found that melanin exerts a profibrotic effect by mediating iron overload and iron death resistance and that inhibition of melanogenesis using ML329 slows KD progression. We did not further explore the impact of intervening in KD by modulating iron overload and iron death or intervening in these abnormal events simultaneously. We will continue to work on the above issues in our subsequent work.

Conclusions

In summary, this study has uncovered intriguing implications for our understanding of skin biology. We found that KD's melanin synthesis pathway is abnormally activated in melanocytes, leading to the translocation of melanin to the deeper dermal layers of the skin. This process induces further the proliferation, migration, and collagen deposition of fibroblasts, which are iron-overloading- and ferroptosis resistance-dependent. The study also revealed that melanin maintains the proliferation-independent immortality property of melanocytes in an autocrine manner. Melanin in the epidermis could further enhance the expression of keratinocyte PAR-2 and facilitate its transfer to superficial layers of the skin, which may be related to skin color deepening. The pharmacological inhibition of melanin synthesis by ML329 has been shown to alleviate KD in mice, suggesting potential therapeutic implications for these findings.

Abbreviations

KD	Keloid
KN	KD neighboring normal control subjects
FDA	Food and Drug Administration
CFDA	China Food and Drug Administration
MITF	Microphthalmia-associated transcription factor
TYR	Tyrosinase
TRP-1/TYRP1	Tyrosinase-related protein-1
TRP-2/TYRP2	Tyrosinase-related protein-2
PAR-2	Proteinase-activating receptor
Pmel17	Premelanosomal protein 17
scRNA-seq	Single-cell RNA sequencing
UMAP	Uniform manifold approximation and projection
MLANA	Melanoma antigen recognized by T-cells 1
KEGG	The Kyoto Encyclopedia of Genes and Genomes
GO	Gene Ontology
KASI	The Keloid Area and Severity Index
qPCR	quantitative Real-time PCR
DEGs	Differentially Expressed Genes
HE	Hematoxylin-Eosin
pHEMs	Primary human epidermal melanocytes
IHC	Immunohistochemistry
S100A9	S100 calcium binding protein A9
S100A8	S100 calcium binding protein A8
S100A4	S100 calcium binding protein A4
α-SMA	Anti-smooth muscle antibody
COL1A1	Collagen type I alpha 1 chain

COL1A2	Collagen type I alpha 2 chain
COL3A1	Collagen type III alpha 1 chain
IL-17	Interleukin-17
TNF-α	Tumor Necrosis Factor-alpha
CCL2	Chemokine (C-C motif) ligand 2
JUN	Jun Proto-Oncogene
FOS	Fos Proto-Oncogene
TNFSF10	Tumor necrosis factor superfamily member
NFKBIA	Nuclear factor of kappa light polypeptide gene enhancer in B-cells inhibitor alpha
CLDN1	Claudin1
ACTG1	Actin gamma 1
ACTN4	Actinin alpha 4
ELISA	Enzyme-Linked Immunosorbent Assay
KRT15	Keratin 15
COL17A1	Collagen type (1:100) alpha 1 chain
NC	Negative control PI3K, Phosphatidylinositol 3-kinase
AKT	Protein Kinase B
ECM	Extracellular Matrix
FTH1	Ferritin heavy chain 1
FTL	Ferritin light chain
TFRC	Transferrin receptor
SLC40A1/FPN1	Solute carrier family 40 member 1
FAC	Ferric citrate
DFO	Deferoxamine
GPX4	Glutathione peroxidase 4
SLC3A2	Solute carrier family 3 member 2
SLC7A11	Solute carrier family 7 member 11
ACSL4	Acyl-CoA synthetase long-chain family member 4
4-HNE	4-Hydroxynonenal
MDA	Malondialdehyde
CCK8	Cell Counting Kit-8
c-Kit/CD117	Receptor tyrosine kinase
ROS	Reactive Oxygen Species

Supplementary Information

The online version contains supplementary material available at https://doi.org/10.1186/s12964-025-02116-z.

Supplementary Material 1

Supplementary Material 2

Acknowledgements
This study was supported by the Human Phenome Data Center of Fudan university.

Author contributions
XX conducted experiments and collected and mined data. YX analyzed and interpreted data. YZ, YG, YC, CS, YM, ZX, WW, MS, YY, JL, JH, ML, and WW analyzed the results. XS designed the conception and experiment, supervised the study, and wrote the manuscript. All authors read and approved the final manuscript.

Funding
This work was supported by the National Science Foundation of China (82270070, 82030003, 81903203, 82373507, and 82173442); National Key Research and Development Program of China (2023YFC2507102); Young clinical full-time research team training program (DGF828024-3/007); CAMS Innovation Fund for Medical Sciences (2019-I2M-5-066); the Shanghai Municipal Science and Technology Major Project (2017SHZDZX01); Shanghai Engineering Research Center of Hair Medicine (19DZ2250500), Leading Talent Project of Shanghai Health Commission (2022LJ017), Jing'an District Clinical Advantage Special Disease Construction Project (2021ZB01), Clinical Research Plan of SHDC (SHDC22022302), Shanghai Municipal Commission of Health and Family Planning (2023ZZ02018), and Shanghai Municipal Key Clinical Specialty (shslczdzk01002).

Data availability
No datasets were generated or analysed during the current study.

Declarations

Ethics approval and consent to participate
Every animal experiment complied with the regulations authorized by Fudan University's Institutional Animal Care and Use Committee (Approval number. FE20002). Every experiment involving human subjects complied with the ethical guidelines and protocols authorized by Fudan University's School of Life Sciences ethics committee (Approval no. KY2023-015). Before beginning the study, each participant received information about it and completed informed consent papers.

Consent for publication
All authors have agreed to publish this manuscript.

Competing interests
The authors declare no competing interests.

Author details
[1]Department of Dermatology, Huashan Hospital, Fudan University, Shanghai, China
[2]School of Life Science and Human Phenome Institute, Fudan University, Shanghai, China
[3]Department of Thoracic Surgery, Huashan Hospital & Cancer Metastasis Institute, Fudan University, Shanghai, China
[4]Deptartment of Allergy and Immunology, Huashan Hospital, and Research Center of Allergy and Diseases, Fudan University, Shanghai, China
[5]Research Unit of Dissecting the Population Genetics and Developing New Technologies for Treatment and Prevention of Skin Phenotypes and Dermatological Diseases (2019RU058), Chinese Academy of Medical Sciences, Shanghai, China
[6]Department of Dermatology, State Key Laboratory of Molecular Engineering of Polymers, Shanghai Institute of Dermatology, Huashan Hospital, Jing'an District Central Hospital, Fudan University, Shanghai, China
[7]National Clinical Research Center for Aging and Medicine, Huashan Hospital, Fudan University, Shanghai 200040, China
[8]Academy for Engineering and Technology, Fudan University, Shanghai 200433, China

Received: 24 October 2024 / Accepted: 20 February 2025
Published online: 18 March 2025

References

1. Al-Attar A, Mess S, Thomassen JM, Kauffman CL, Davison SP. Keloid pathogenesis and treatment. Plast Reconstr Surg. 2006;117:286–300.
2. Wang Y, Chen Y, Wu J, Shi X. BMP1 promotes keloid by inducing fibroblast inflammation and fibrogenesis. J Cell Biochem. 2024;125:e30609.
3. Direder M, Weiss T, Copic D, Vorstandlechner V, Laggner M, Pfisterer K, Mildner CS, Klas K, Bormann D, Haslik W, et al. Schwann cells contribute to keloid formation. Matrix Biol. 2022;108:55–76.
4. Ogawa R. Keloid and hypertrophic scars are the result of chronic inflammation in the reticular dermis. Int J Mol Sci. 2017;18(3):606.
5. Liu J, Huang Y, Gong Y, Liu Q, Lin J, Liu J, Liu M, Huang J, Pu W, Ma Y, et al. CTHRC1 + fibroblasts are stimulated by macrophage-secreted SPP1 to induce excessive collagen deposition in keloids. Clin Transl Med. 2022;12:e1115.
6. Liu X, Chen W, Zeng Q, Ma B, Li Z, Meng T, Chen J, Yu N, Zhou Z, Long X. Single-Cell RNA-Sequencing reveals Lineage-Specific regulatory changes of fibroblasts and vascular endothelial cells in keloids. J Invest Dermatol. 2022;142:124–e135111.
7. Shim J, Oh SJ, Yeo E, Park JH, Bae JH, Kim SH, Lee D, Lee JH. Integrated analysis of Single-Cell and Spatial transcriptomics in keloids: highlights on fibrovascular interactions in keloid pathogenesis. J Invest Dermatol. 2022;142:2128–e21392111.
8. Deng CC, Hu YF, Zhu DH, Cheng Q, Gu JJ, Feng QL, Zhang LX, Xu YP, Wang D, Rong Z, Yang B. Single-cell RNA-seq reveals fibroblast heterogeneity and increased mesenchymal fibroblasts in human fibrotic skin diseases. Nat Commun. 2021;12:3709.
9. Direder M, Wielscher M, Weiss T, Laggner M, Copic D, Klas K, Bormann D, Vorstandlechner V, Tschachler E, Jan Ankersmit H, Mildner M.

The transcriptional profile of keloidal Schwann cells. Exp Mol Med. 2022;54:1886–900.
10. Hampton G, Kim J, Edwards TL, Hellwege JN, Velez Edwards DR. Uterine leiomyomata and keloids fibrosis origins: a mini-review of fibroproliferative diseases. Am J Physiol Cell Physiol. 2023;325:C817–22.
11. Limandjaja GC, Niessen FB, Scheper RJ, Gibbs S. The keloid disorder: heterogeneity, histopathology, mechanisms and models. Front Cell Dev Biol. 2020;8:360.
12. Huang C, Wu Z, Du Y, Ogawa R. The Epidemiology of Keloids. In Textbook on Scar Management: State of the Art Management and Emerging Technologies. Edited by Teot L, Mustoe TA, Middelkoop E, Gauglitz GG. Cham (CH). 2020:29–35.
13. D'Mello SA, Finlay GJ, Baguley BC, Askarian-Amiri ME. Signaling pathways in melanogenesis. Int J Mol Sci 2016;17(7):1144.
14. Vachtenheim J, Borovansky J. Transcription physiology of pigment formation in melanocytes: central role of MITF. Exp Dermatol. 2010;19:617–27.
15. Raposo G, Marks MS. Melanosomes–dark organelles enlighten endosomal membrane transport. Nat Rev Mol Cell Biol. 2007;8:786–97.
16. Kipouros I, Stanczak A, Ginsbach JW, Andrikopoulos PC, Rulisek L, Solomon EI. Elucidation of the tyrosinase/O(2)/monophenol ternary intermediate that dictates the monooxygenation mechanism in melanin biosynthesis. Proc Natl Acad Sci U S A. 2022;119:e2205619119.
17. Kawahara R, Usami T, Arakawa S, Kamo H, Suzuki T, Komatsu R, Hara H, Niwa Y, Shimizu E, Dohmae N, et al. Biogenesis of fibrils requires C-mannosylation of PMEL. FEBS J. 2023;290:5373–94.
18. Moreiras H, Seabra MC, Barral DC. Melanin transfer in the epidermis: the pursuit of skin pigmentation control mechanisms. Int J Mol Sci. 2021;22(9):4466.
19. Bento-Lopes L, Cabaco LC, Charneca J, Neto MV, Seabra MC, Barral DC. Melanin's journey from melanocytes to keratinocytes: Uncovering the Molecular Mechanisms of Melanin Transfer and Processing. Int J Mol Sci. 2023;24(14):11289.
20. Wihastyoko HYL, Perdanakusuma DS, Soeharto S, Widjajanto E, Handono K, Pardjianto B. Correlation of melanin content with collagen density in keloid patients. Open Access Macedonian J Med Sci. 2021;9:265–71.
21. Oei F, Putra IB, Jusuf NK. The relationship between skin color and keloid. Bali Med J. 2021;10:835–8.
22. Shen Z, Shao J, Sun J, Xu J. Exosomes released by melanocytes modulate fibroblasts to promote keloid formation: a pilot study. J Zhejiang Univ Sci B. 2022;23:699–704.
23. Surbek M, Sukseree S, Eckhart L. Iron metabolism of the skin: recycling versus release. Metabolites 2023;13(9):1005.
24. Gao X, Song Y, Wu J, Lu S, Min X, Liu L, Hu L, Zheng M, Du P, Yu Y et al. Iron-dependent epigenetic modulation promotes pathogenic T cell differentiation in lupus. J Clin Invest 2022;132(9):e152345.
25. Li S, Luo X, Zhang S, Su Y, Deng M, Zhu Y, Zhang P, Wu R, Zhao M. Ferroptosis activation contributes to the formation of skin lesions in psoriasis vulgaris. Antioxid (Basel) 2023;12(2):310.
26. Ubellacker JM, Tasdogan A, Ramesh V, Shen B, Mitchell EC, Martin-Sandoval MS, Gu Z, McCormick ML, Durham AB, Spitz DR, et al. Lymph protects metastasizing melanoma cells from ferroptosis. Nature. 2020;585:113–8.
27. Zhang F, Xiao Y, Huang Z, Wang Y, Wan W, Zou H, Wang B, Qiu X, Yang X. Upregulation of GPX4 drives ferroptosis resistance in scleroderma skin fibroblasts. Free Radic Biol Med. 2024;221:23–30.
28. Shou Y, Yang L, Yang Y, Xu J. Inhibition of keratinocyte ferroptosis suppresses psoriatic inflammation. Cell Death Dis. 2021;12:1009.
29. Feng Z, Qin Y, Huo F, Jian Z, Li X, Geng J, Li Y, Wu J. NMN recruits GSH to enhance GPX4-mediated ferroptosis defense in UV irradiation induced skin injury. Biochim Biophys Acta Mol Basis Dis. 2022;1868:166287.
30. Ogawa R. Japan Scar Workshop (JSW) Scar Scale (JSS) for Assessing Keloids and Hypertrophic Scars. In *Textbook on Scar Management: State of the Art Management and Emerging Technologies.* Edited by Teot L, Mustoe TA, Middelkoop E, Gauglitz GG. Cham (CH); 2020: 133–140.
31. Limmer EE, Kerby E, Lies S, Limmer B, Limmer R, Teske N, Savory S, Reisch JS, Glass DA. 2nd: the keloid area and severity index (KASI): an objective tool for the evaluation of keloids. Br J Dermatol. 2022;187:799–800.
32. Chung S, Lim GJ, Lee JY. Quantitative analysis of melanin content in a three-dimensional melanoma cell culture. Sci Rep. 2019;9:780.
33. Yang Y, Luo M, Zhang K, Zhang J, Gao T, Connell DO, Yao F, Mu C, Cai B, Shang Y, Chen W. Nedd4 ubiquitylates VDAC2/3 to suppress erastin-induced ferroptosis in melanoma. Nat Commun. 2020;11:433.
34. Li C, Liu J, Hou W, Kang R, Tang D. STING1 promotes ferroptosis through MFN1/2-Dependent mitochondrial fusion. Front Cell Dev Biol. 2021;9:698679.
35. He Y, Tsou PS, Khanna D, Sawalha AH. Methyl-CpG-binding protein 2 mediates antifibrotic effects in scleroderma fibroblasts. Ann Rheum Dis. 2018;77:1208–18.
36. Chen Y, Gong Y, Shi M, Zhu H, Tang Y, Huang D, Wang W, Shi C, Xia X, Zhang Y et al. miR-3606-3p alleviates skin fibrosis by integratively suppressing the integrin/fak, p-AKT/p-ERK, and TGF-beta signaling cascades. J Adv Res. 2024;20:S2090–1232(24)00546-0.
37. Manetti M, Romano E, Rosa I, Guiducci S, Bellando-Randone S, De Paulis A, Ibba-Manneschi L, Matucci-Cerinic M. Endothelial-to-mesenchymal transition contributes to endothelial dysfunction and dermal fibrosis in systemic sclerosis. Ann Rheum Dis. 2017;76:924–34.
38. Scott G, Leopardi S, Printup S, Malhi N, Seiberg M, Lapoint R. Proteinase-activated receptor-2 stimulates prostaglandin production in keratinocytes: analysis of prostaglandin receptors on human melanocytes and effects of PGE2 and PGF2alpha on melanocyte dendricity. J Invest Dermatol. 2004;122:1214–24.
39. Wu Q, Carlos AR, Braza F, Bergman ML, Kitoko JZ, Bastos-Amador P, Cuadrado E, Martins R, Oliveira BS, Martins VC, et al. Ferritin heavy chain supports stability and function of the regulatory T cell lineage. EMBO J. 2024;43:1445–83.
40. Lee A, Lim J, Lim JS. Emerging roles of MITF as a crucial regulator of immunity. Exp Mol Med. 2024;56:311–8.
41. Collin J, Hasoon MSR, Zerti D, Hammadi S, Dorgau B, Clarke L, Steel D, Hussain R, Coxhead J, Lisgo S, et al. Single-cell RNA sequencing reveals transcriptional changes of human choroidal and retinal pigment epithelium cells during fetal development, in healthy adult and intermediate age-related macular degeneration. Hum Mol Genet. 2023;32:1698–710.
42. Nagatsu T, Nakashima A, Watanabe H, Ito S, Wakamatsu K. Neuromelanin in parkinson's disease: Tyrosine hydroxylase and tyrosinase. Int J Mol Sci. 2022;23(8):4176.
43. Yan J, Ji Y, Zhang P, Lu X, Fan Q, Pan D, Yang R, Xu Y, Wang L, Zhang L, Yang M. Melanin nanoparticles as an endogenous agent for efficient iron overload therapy. J Mater Chem B. 2016;4:7233–40.
44. Yang L, Li X, Wang Y. Ferrostatin-1 inhibits fibroblast fibrosis in keloid by inhibiting ferroptosis. PeerJ. 2024;12:e17551.
45. Zhang J, Liu L, Li X, Shen X, Yang G, Deng Y, Hu Z, Zhang J, Lu Y. 5-ALA-PDT induced ferroptosis in keloid fibroblasts via ROS, accompanied by downregulation of xCT, GPX4. Photodiagnosis Photodyn Ther. 2023;42:103612.
46. Viceconte N, Burguillos MA, Herrera AJ, De Pablos RM, Joseph B, Venero JL. Neuromelanin activates Proinflammatory microglia through a caspase-8-dependent mechanism. J Neuroinflammation. 2015;12:5.
47. Cichorek M, Wachulska M, Stasiewicz A, Tyminska A. Skin melanocytes: biology and development. Postepy Dermatol Alergol. 2013;30:30–41.
48. Shaheen AA. Risk factors of keloids: A mini review. Austin J Dermat. 2017;4(2):1074. https://doi.org/10.26420/austinjdermatolog.2017.1074
49. Bucak IH, Almis H, Benli S, Turgut M. The assessment of skin color and Iron levels in pediatric patients with beta-Thalassemia major using a visual skin color chart. Hemoglobin. 2017;41:120–3.
50. Zhang Y, Zhou S, Kai Y, Zhang YQ, Peng C, Li Z, Mughal MJ, Julie B, Zheng X, Ma J, et al. O-GlcNAcylation of MITF regulates its activity and CDK4/6 inhibitor resistance in breast cancer. Nat Commun. 2024;15:5597.
51. Chen Y, Wang C, Wu Y, Wang Y, Meng Y, Wu F, Zhang H, Cheng YY, Jiang X, Shi J et al. Nutrient-delivery and metabolism reactivation therapy for melanoma. Nat Nanotechnol. 2024;19(9):1399–1408.

Publisher's note